# Pressure swing adsorption cycle design for ethylene/ethane separation process

Balan Ramani **(TU Delft)**

October 2015
ECN-O--15-042

Supervised by:
Jurriaan Boon (ECN)
Wim Buijs (TU Delft)

# Acknowledgement

I would like to sincerely thank my supervisor at ECN, Jurriaan Boon, and my supervisor at Delft University of Technology Prof. Wim Buijs for their help in completing this project. I am very impressed by the competence and knowledge Jurriaan had shown during the internship period and his quick feedback. The regular progress meeting with him helped me progress through my work much faster. I want to thank Paul Cobden, Jan Wilco Dijkstra, Marija Sarić, Eric van Dijk and all the researchers at Sustainable Process Technology department, ECN for their help and for all the interesting conversations I had with them during the internship period.


# Abstract


Olefin from Paraffin Extraction by Reversible Adsorption (OPERA) is a pressure swing based adsorption concept proposed to separate ethylene (C2H4) from ethane (C2H6) and propylene (C3H6) using zeolite 13X sorbent, as an alternate method to the energy intensive cryogenic distillation process. OPERA is a cyclic process, that comprises high pressure adsorption and rinse, pressure equalisation and low pressure purge. An extensive parameter study based on numerical simulations is made to observe the effects of various factors on the performance parameters (purity and recovery of C2H4). An optimised OPERA cycle is designed considering the observed effects from the parameter study. The proposed cycle is able to produce 99.7% pure ethylene with 19% recovery. The system uses five pressure equalisations and requires 9 columns. Preliminary economic analysis indicates that installing an OPERA cycle operating for the given conditions between 30 bar and 1 bar at 80 °C in the upstream of the cryogenic distillation column actually increases the overall energy consumption of the separation process.

# Contents

# Summary

The objective of this project is to reduce the high energy consumption involved in the operation of the cryogenic distillation system of the Naphtha cracking process for the separation of ethylene from ethane by installing a multi-step pressure swing based adsorption cycle in the upstream of the cryogenic distillation system.

An isotherm is plotted using Zeolite 13X sorbent considering the effects of propylene in addition to ethane on ethylene's purity and recovery.

First, an equilibrium based PSA model is developed using the above isotherm to approximately estimate the dimensions of the adsorption column and the corresponding amount of sorbent needed. Also, the purity and recovery of $C_2H_4$ attainable through the equilibrium effects without involving the kinetic effects are studied.

A numerical model of the PSA system operating at 80 °C between 30 bar and 1 bar is developed involving the kinetic effects. An extensive parameter study is performed to observe the effects of various factors on the performance parameters i.e. the purity and recovery of $C_2H_4$ product.

An optimised cycle is designed considering the effects observed from the parameter study to produce high purity $C_2H_4$ product with maximum possible recovery.

Preliminary analysis indicates that installing an OPERA system upstream with 60% $C_2H_4$ adsorption from the feed stream can reduce the energy consumption of cryogenic distillation up to 65%. But the energy required for $C_2H_4$ rinse gas compression is much higher than the saving made. Also, the $C_2H_4$ recovery from OPERA system is very low (19 wt.%) for operating between 30 bar and 1 bar at 80 °C .

# 1

# Introduction

Ethylene ($C_2H_4$) is the most important organic chemical with an annual global production of over 75 million tonne exceeding that of any other organic compound **Fout! Verwijzingsbron niet gevonden.**. Ethene is the building block for a vast range of chemicals from plastics to antifreeze solutions and solvents.

The diagram below **Figure** 1 summarizes and gives an indication of the many industrial ethylene made substances.

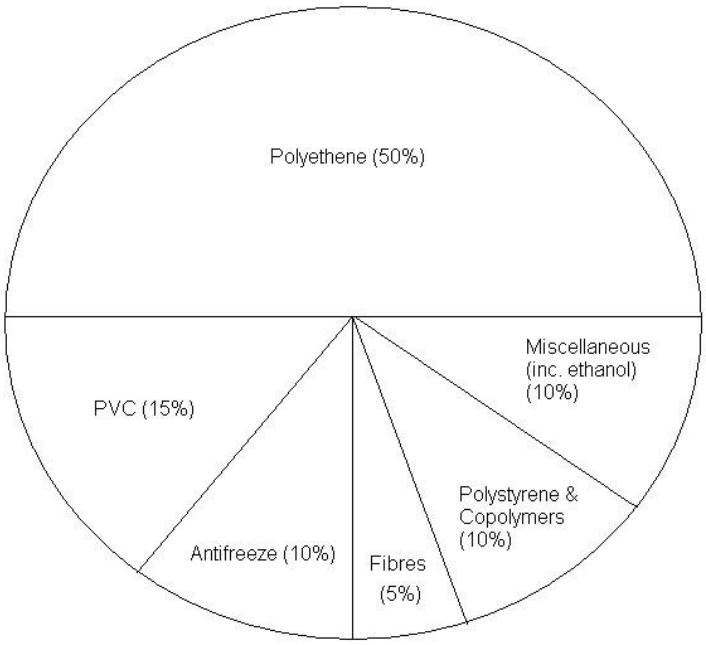


Figure 1: Uses of ethylene/proportions of synthetic organic chemicals which are made from ethylene [13]

## 1.1 Production Process

Ethylene is produced commercially by the steam cracking of a wide range of hydrocarbon feed stocks. Ethylene is obtained in the $C_2$ splitter from the ethylene/ethane mixture.

Currently the separation of ethylene/ethane mixture is performed at high pressure in large and tall cryogenic distillation columns as shown in **Figure** 2. The small difference in relative volatility between ethylene and ethane ($\alpha < 1.5$) makes it a very energy intensive process. Distillation is the largest energy consumer within the chemical industry. The annual worldwide energy demand for olefin/paraffin separation is over 300 PJ for approximately 130 million tonne of olefin. Besides the high energy demands, the safety requirement for cryogenic distillation will also be very demanding, since the flammable compressed and cooled liquefied gas could explode in case of cooling failure, in particular since the olefin and paraffin themselves are integrated with the cooling system of the separation process**Fout! Verwijzingsbron niet gevonden.**.

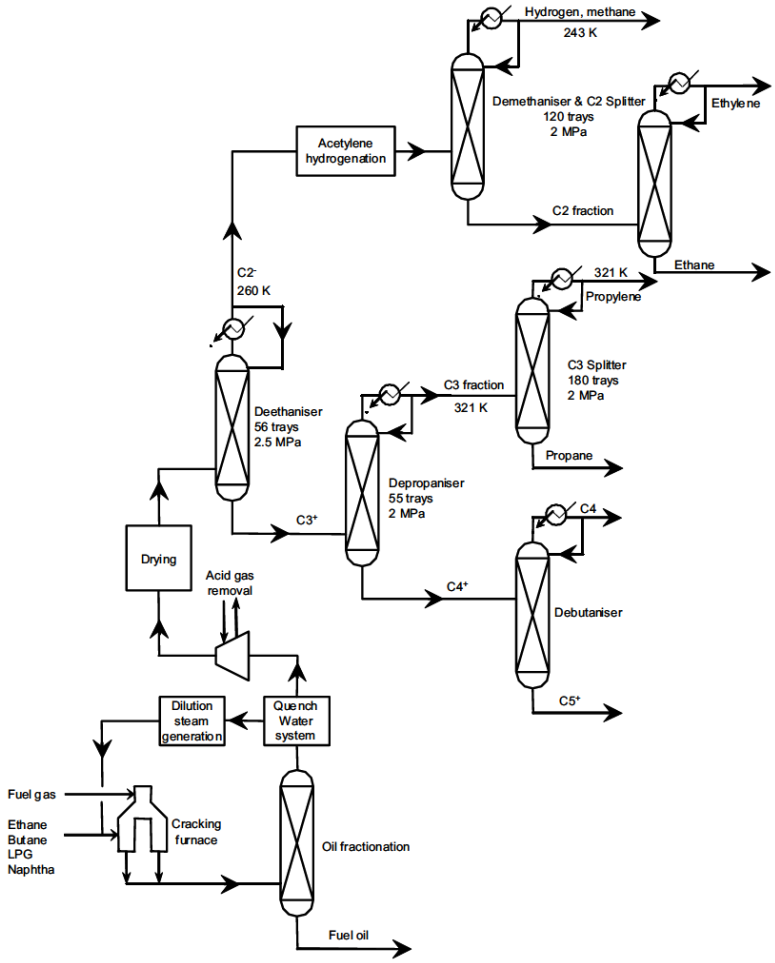


**Figure** 2: Process flow sheet of a typical steam cracking and olefin/paraffin separation plant **Fout! Verwijzingsbron niet gevonden.**

The growing responsibility to reduce the emissions of greenhouse gases resulted in the need to find alternative separation processes to reduce the energy demands. More attention is paid to adsorption aided by a bonding of the olefin, e.g. via π-complexation.

Olefin from Paraffin Extraction by Reversible Adsorption (OPERA) is a pressure swing based adsorption process to separate ethylene from ethane and propylene. The OPERA system is placed upstream to the cryogenic distillation system in order to produce high purity ethylene. So, only the remaining mass flow from the OPERA cycle need to be fed to the cryogenic distillation column with the aim of reducing the high energy consumption involved in the ethylene/ethane distillation process and possibly to increase the throughput of the distillation section.

A numerical model of the OPERA cycle involving high pressure adsorption and rinse, a series of pressure equalisations, depressurisation, low pressure purge and repressurisation steps is developed in the study. A parameter study is performed to observe the effects of various factors on the performance parameters i.e. purity and recovery of $C_2H_4$. Considering the effects of various parameters, an optimised OPERA cycle is designed to produce high purity ethylene.

# 2

# Modelling

## 2.1 Adsorption

In an adsorption process, molecules or atoms or ions in a gas or liquid diffuse to the surface of a solid, where they bond with the solid surface or are held there by weak inter-molecular forces. The adsorbed solute is called the adsorbate, and the solid material is the adsorbent.

To achieve a very large surface area for adsorption per unit volume, highly porous solid adsorbents with small diameter inter-connected pores are used. The porous structures can account for up to 50% of the volume of the material.

During adsorption, the solid adsorbent becomes saturated or nearly saturated with the adsorbate. To recover the adsorbate and allow the adsorbent to be reused, it is regenerated by desorbing the adsorbed substances.

Removal of adsorbates can be generally achieved by changing the pressure or the temperature.

Because the adsorbed component is removed from the solid adsorbent, the adsorbent is said to be "regenerated" and so can be used again to adsorb more adsorbate component from fresh process stream [3].

Adsorption processes can be divided into two groups:

- bulk separation, which involves the separation of up to half of the components from a process stream
- purification, a process in which a small amount of impurity is removed from the gas stream

## 2.2 Adsorbents

Major types of adsorbents in use are:

- Silica gel
- Activated alumina
- Activated carbon
- Carbon molecular sieve
- Zeolites

Most adsorbents are manufactured (such as activated carbons), but a few, such as some zeolites, occur naturally. Each material has its own characteristics such as porosity, pore structure and nature of its adsorbing surfaces.

Pore sizes in adsorbents may be distributed throughout the solid. Pore sizes are classified generally into 3 ranges:

- Macropores have diameters in excess of 50 nm
- Mesopores have diameters in the range of 2 – 50 nm
- Micropores have diameters smaller than 2 nm

Many adsorbent materials, such as carbons, silica gels and alumina, are amorphous and contain complex networks of inter-connected micropores, mesopores and macropores. In contrast, pores in zeolite adsorbents have precise dimensions [3].

### 2.2.1 Zeolites

Zeolites are porous crystalline alumino-silicates which comprise assemblies of $SiO_4$ and $AlO_4$ tetra hydra joined together through the sharing of oxygen atoms.

The general stoichiometric unit cell formula for a zeolite (the framework) is:

$$M_{x/m} [ (AlO_2)_x (SiO_2)_y ] z H_2O \quad (1)$$

where

- M is the cation with valence m
- z is the number of water molecules in each unit cell and
- x and y are integers such that y/x is greater than or equal to 1

Some examples of zeolites are shown in Table 1.

| Framework | Cationic Form | Formula of typical unit cell | Window | Effective channel diameter (nm) |
|---|---|---|---|---|
| | Na | $Na_{12}[(AlO_2)_{12}(SiO_2)_{12}]$ | 8-ring (obstructed) | 0.38 |
| A | Ca | $Ca_2Na_2[(AlO_2)_{12}(SiO_2)_{12}]$ | 8-ring (free) | 0.44 |
| | K | $K_{12}[(AlO_2)_{12}(SiO_2)_{12}]$ | 8-ring (obstructed) | 0.29 |
| | Na | $Na_{86}[(AlO_2)_{86}(SiO_2)_{106}]$ | 12-ring | 0.84 |
| X | Ca | $Ca_{40}Na_6[(AlO_2)_{86}(SiO_2)_{106}]$ | 12-ring | 0.80 |
| | Sr, Ba | $Sr_{21}Ba_{22}[(AlO_2)_{86}(SiO_2)_{106}]$ | 12-ring | 0.80 |
| | Na | $Na_{56}[(AlO_2)_{56}(SiO_2)_{136}]$ | 12-ring | 0.80 |
| Y | K | $K_{56}[(AlO_2)_{56}(SiO_2)_{136}]$ | 12-ring | 0.80 |
| Mordenite | Ag | $Ag_8[(AlO_2)_8(SiO_2)_{40}]$ | 12-ring | 0.70 |
| | H | $H_8[(AlO_2)_8(SiO_2)_{40}]$ | | |
| Silicalite | - | $(SiO_2)_{96}$ | 10-ring | 0.60 |
| ZSM-5 | Na | $Na_3[(AlO_2)_3(SiO_2)_{93}]$ | 10-ring | 0.60 |

**Table** 1: Examples of Zeolite types

The ratio of oxygen atoms to combined aluminium and silicon atoms is always equal to 2, and therefore each aluminium atom introduce a negative charge of one (-1) on the zeolite framework which is balanced by that of an exchangeable cation.

To activate the zeolite, the water molecules are removed by raising the temperature or pulling a vacuum. This resulted in a framework with the remaining atoms spatially intact, producing cavities (known as cages) connected by channels (pores). The channel size is determined by the number of atoms which form the apertures (or windows) leading to the cages. Changing the position and type of the cation changes the channel size and properties of the zeolite, including its selectivity in a given chemical system.

More than 150 synthetic zeolite types are known, the most important commercially being the synthetic types A and X, synthetic mordenite and their ion-exchanged varieties. Of the 40 or so mineral zeolites the most important commercially are chabazite, faujasite and mordenite.

In crystal form, zeolites are distinct from other adsorbents in that, for each type, there is no distribution of pore size. The lattice into which the adsorbate molecules can or cannot enter is precisely uniform. For this reason zeolites are capable of separating effectively on the basis of size and they are often known as molecular sieves.

In addition to changes to the cationic structure, the Si/Al ratio can be varied, thus zeolites with widely different adsorptive properties may be tailored by the appropriate choice of framework structure, cationic form, and silica-to-alumina ratio in order to achieve the selectivity required for a given separation.

The ionic nature of most zeolites means that they have a high affinity for water and other polar molecules such as hydrogen sulphide. However, as the silica-to-alumina ratio is increased the material can become hydrophobic. Such zeolites can be used in the removal of volatile organic compounds from air [3].

### 2.2.2 Selection of Zeolite 13X as sorbent for OPERA process

Zeolite 13X (NaX Faujasite) has large pore size for kinetics. Also, the $Na^+$ ions aid π-bonding thereby increasing the selectivity of olefin ($C_2H_4$) over paraffin ($C_2H_6$) which is discussed in detail in Chapter 2.5. Considering these reasons, Zeolite 13X is chosen as the sorbent for the OPERA process.

## 2.3 Physical Adsorption and Chemical Adsorption

The phenomenon of adsorption is essentially an attraction of adsorbate molecules to an adsorbent surface. The preferential concentration of molecules in the proximity of a surface arises because of the presence of the surface forces on an adsorbent solid. Adsorption is always an exothermic process.

We can distinguish between two types of adsorption process depending on which of these two force types plays the bigger role in the process. Adsorption processes can be classified as either physical adsorption (van der Waals adsorption) or chemisorption (activated adsorption) depending on the type of forces between the adsorbate and the adsorbent.

In physical adsorption, the individuality of the adsorbate and the adsorbent are preserved. In chemisorption, there is a transfer or sharing of electron, or breakage of the adsorbate into atoms or radicals which are bound separately.

Physical adsorption from a gas occurs when the inter-molecular attractive forces between molecules of the solid adsorbent and the gas are greater than those between molecules of the gas itself. In effect, the resulting adsorption is like condensation, which is exothermic and thus is accompanied by the release of heat.

Physical adsorption occurs quickly and may be mono-molecular layer, or two, three or more layers thick (multi-molecular). As physical adsorption takes place, it begins as a monolayer. It can then become multi-layer, and then, if the pores are close to the size of the molecules, more adsorption occurs until the pores are filled with adsorbate. Accordingly, the maximum capacity of a porous adsorbent can be more related to the pore volume than to the surface area.

In contrast, chemisorption involves the formation of chemical bonds between the adsorbate and adsorbent in a monolayer, often with a release of heat much larger than the heat of condensation. Chemisorption from a gas generally takes place only at temperatures greater than 200 °C, and may be slow and irreversible [3].

Most commercial adsorbents rely on physical adsorption as it is comparatively fast and reversible.

## 2.4 Adsorption Isotherm

The process of adsorption is usually studied through graphs know as adsorption isotherm. It is the graph between the amounts of adsorbate (x) adsorbed on the surface of adsorbent (m) and pressure at constant temperature as shown in **Figure** 3.

In the process of adsorption, adsorbate gets adsorbed on adsorbent.

(2)

$$\text{Adsorbate} + \text{Adsorbent} \underset{\text{desorption}}{\overset{\text{Adsorption}}{\rightleftharpoons}} \text{Adsorption}$$

According to Le Chatelier's principle, in case of application of excess of pressure to the equilibrium system, the equilibrium will shift in the direction where the number of molecules in the gas phase decreases. Since number of molecules decreases in forward direction, with the increases in pressure, forward direction of equilibrium will be favored.

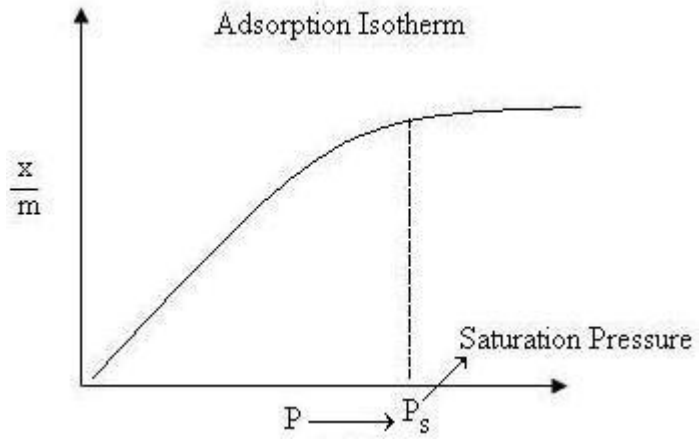


**Figure** 3: Basic Adsorption Isotherm [3]

From the graph, we can predict that after saturation pressure ($P_s$), adsorption does not occur anymore. This can be explained by the fact that there are limited numbers of vacancies on the surface of the adsorbent. At high pressure a stage is reached when all the sites are occupied and further increase in pressure does not cause any difference in adsorption process.

## 2.4.1 Langmuir Adsorption Isotherm

This isotherm is based on different assumptions one of which is that dynamic equilibrium exists between adsorbed gaseous molecules and the free gaseous molecules[3].

$$A(g) + B(S) \underset{\text{desorption}}{\overset{\text{Adsorption}}{\rightleftharpoons}} AB \qquad (3)$$

Where

A(g) is unadsorbed gaseous molecule,
B(s) is unoccupied metal surface and
AB is adsorbed gaseous molecule.

Based on his theory, he derived Langmuir equation which depicted a relationship between the number of active sites of the surface undergoing adsorption and pressure.

$$\theta = \frac{KP}{1+KP} \qquad (4)$$

Where

θ is the number of sites of the surface which are covered with gaseous molecule,
P is the pressure and
K is the equilibrium constant for distribution of adsorbate between the surface and the gas phase.

At lower pressure, KP is so small, that factor (1+KP) in denominator can almost be ignored. So Langmuir equation reduces to form linear isotherm equation (Henry's law)

$$\theta = KP \tag{5}$$

At high pressure KP is so large, that factor (1+KP) in denominator is nearly equal to KP. So Langmuir equation reduces to

$$\theta = \frac{KP}{KP} = 1 \tag{6}$$

## 2.5 OPERA Isotherm

For the adsorption of pure gases, various single component models have been proposed to describe the adsorption loadings at different pressures and temperatures. For the adsorption of multicomponent gas mixtures like the olefin/paraffin separation, the single component models can be extended to include the influence of other components on the adsorption behaviour of each individual component. The single component Dual Site Langmuir (DSL) isotherm is extended to a multi-component isotherm. The adsorption capacity of component i in a mixture of N components is then determined via the following equation **Fout! Verwijzingsbron niet gevonden.**:

$$q_i = \left(\frac{q_{i,sat}\, b_i\, p_i}{1+\Sigma_{j=1}^{N} b_j\, p_j}\right)_A + \left(\frac{q_{i,sat}\, b_i\, p_i}{1+\Sigma_{j=1}^{N} b_j\, p_j}\right)_B \tag{7}$$

Where $b_i$ is the adsorption equilibrium constant and is defined as

$$b_i = b_{i,inf}\ \exp\left(\frac{-\Delta H_i}{R_g T}\right) \tag{8}$$

Where

P = pressure, bar
T = temperature, K
$p_i$ = partial pressure of component i in the feed, bar
$q_i$ = adsorbed phase concentration of component i, mol $kg^{-1}$
$q_{i,sat}$ = saturation limit of adsorbed phase concentration of component i, mol $kg^{-1}$
$b_i$ = adsorption equilibrium constant, $bar^{-1}$
$b_{i,inf}$ = pre-exponential factor, $bar^{-1}$
$\Delta H_i$ = enthalpy change on adsorption, kJ $mol^{-1}$
$R_g$ = universal gas constant, $R_g$=8.314 J $mol^{-1}$ $K^{-1}$

The parameters for the DSL isotherm model for zeolite 13X are taken from literature **Fout! Verwijzingsbron niet gevonden.**. Only ethylene, ethane and propylene are assumed to adsorb.

| Parameter | Value | |
|---|---|---|
| $q_{C2H4,sat\_A}$ | 2.91 | mol.$kg^{-1}$ |
| $q_{C2H6,sat\_A}$ | 3.93 | mol.$kg^{-1}$ |

| | | |
|---|---|---|
| $q_{C3H6,sat\_A}$ | 2.71 | $mol.kg^{-1}$ |
| $q_{C2H4,sat\_B}$ | 1.58 | $mol.kg^{-1}$ |
| $q_{C2H6,sat\_B}$ | 0 | $mol.kg^{-1}$ |
| $q_{C3H6,sat\_B}$ | 1.14 | $mol.kg^{-1}$ |
| $b_{C2H4,inf\_A}$ | $3.14 \times 10^{-5}$ | $bar^{-1}$ |
| $b_{C2H6,inf\_A}$ | $1.02 \times 10^{-4}$ | $bar^{-1}$ |
| $b_{C3H6,inf\_A}$ | $1.52 \times 10^{-4}$ | $bar^{-1}$ |
| $b_{C2H4,inf\ B}$ | $1.71 \times 10^{-5}$ | $bar^{-1}$ |
| $b_{C2H6,inf\_B}$ | 0 | $bar^{-1}$ |
| $b_{C3H6,inf\_B}$ | $1.25 \times 10^{-7}$ | $bar^{-1}$ |
| $-\Delta H_{C2H4\_A}$ | 37 | $kJ.mol^{-1}$ |
| $-\Delta H_{C2H6\ A}$ | 26.5 | $kJ.mol^{-1}$ |
| $-\Delta H_{C3H6\_A}$ | 39.82 | $kJ.mol^{-1}$ |
| $-\Delta H_{C2H4\_B}$ | 30.11 | $kJ.mol^{-1}$ |
| $-\Delta H_{C2H6\_B}$ | 0 | $kJ.mol^{-1}$ |
| $-\Delta H_{C3H6\_B}$ | 50.2 | $kJ.mol^{-1}$ |

**Table** 2: Parameters for DSL Isotherm Model

The above described DSL model is used to test the adsorptive capacity of $C_2H_4$ over other components at positions (I) and (II)

### 2.5.1 Case (I): After Acetylene ($C_2H_2$) convertor

The condition and composition of the stream after $C_2H_2$ convertor are as shown in **Table** 3 and **Table** 4 respectively

| Parameter | Value | |
|---|---|---|
| P | 30 | bar |
| T | 80 | °C |
| $F_m$ | 45.2 | kg/s |

**Table** 3: Stream condition after $C_2H_2$ convertor

| Components | Composition (wt%) |
|---|---|
| $H_2$ | 0.001 |
| CO | 0.0005 |
| $CH_4$ | 0.2974 |
| $C_2H_4$ | 0.5987 |
| $C_2H_6$ | 0.1008 |
| $C_3H_6$ | 0.0016 |

**Table** 4: Stream composition after $C_2H_2$ convertor

Using the DSL model described above for Zeolite 13X, the adsorption isotherm for the stream after $C_2H_2$ convertor is plotted as follows:

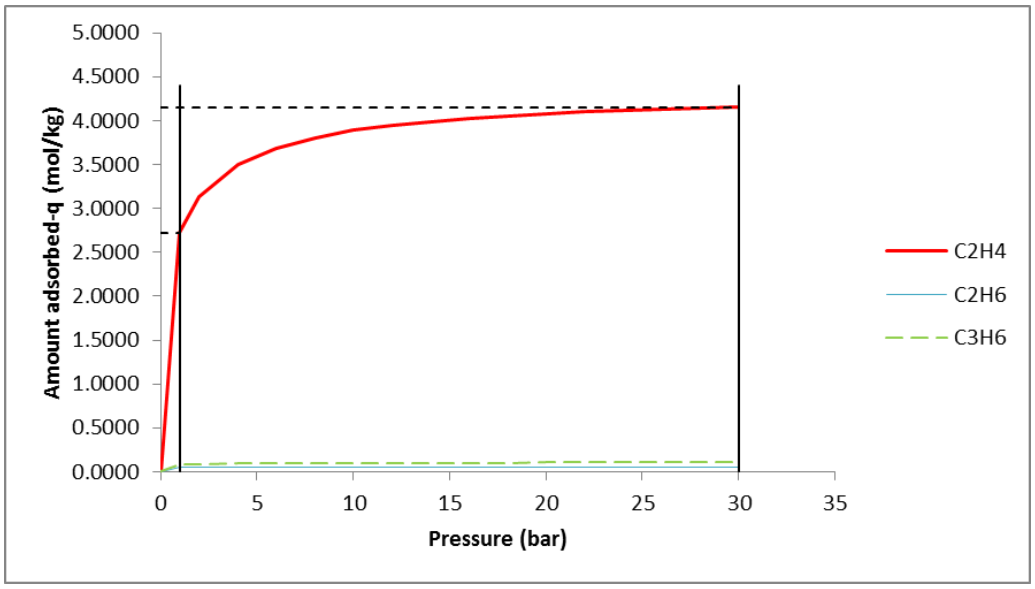


**Figure** 4: Adsorption Isotherm for stream composition after Acetylene ($C_2H_2$) converter

## 2.5.2 Case (II): before $C_2$ ($C_2H_4/C_2H_6$) splitter

The condition and composition of the stream before $C_2$ splitter are as shown in **Table** 5 and **Table** 6 respectively.

| Parameters | Value | |
|---|---|---|
| P | 25 | bar |
| T | -8 | °C |
| $F_m$ | 31.5 | kg/s |

**Table** 5: Stream condition before $C_2$ splitter

| Components | Composition (wt. %) |
|---|---|
| $C_2H_4$ | 0.8535 |
| $C_2H_6$ | 0.1442 |
| $C_3H_6$ | 0.0023 |

**Table** 6: Stream composition before $C_2$ splitter

Using the DSL model described above for Zeolite 13X, the adsorption isotherm for the stream before $C_2$ splitter is plotted as follows:

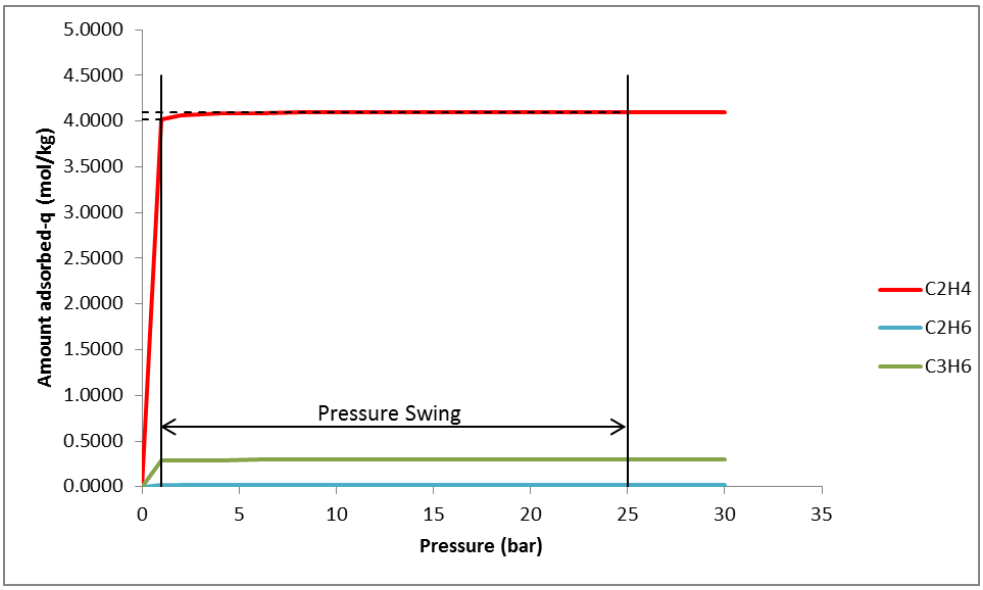


**Figure** 5: Adsorption Isotherm for stream composition before $C_2$ splitter

The working capacity i.e. the amount of moles adsorbed per unit weight of the adsorbent and the selectivity of $C_2H_4$ over other components for both positions (I) and (II) are summarised in **Table** 7 as follows:

| Parameters | | After $C_2H_2$ convertor | Before $C_2$ splitter |
|---|---|---|---|
| Working capacity (mol/kg) | | 1.4287 | 0.0842 |
| Selectivity | $C_2H_4/C_2H_6$ | 178 | 2859 |
| | $C_2H_4/C_3H_6$ | 55 | 8 |
| | $C_2H_4/(C_2H_6\&C_3H_6)$ | 42 | 8 |

**Table** 7: Comparison of Zeolite 13X adsorption isotherms after $C_2H_2$ convertor and before $C_2$ splitter

From the results summarised in **Table** 7 we can clearly see that the stream after $C_2H_2$ convertor has better working capacity as well as selectivity for $C_2H_4$ over other components on Zeolite 13X adsorbent. Note that the performance of the PSA system could be improved by operating at higher temperature (using an additional heat exchanger). The effect of temperature on the PSA cycle is discussed below.

**Effect of Temperature on Adsorption Isotherm**

A study is performed to observe the effects of Temperature variation on Adsorption Isotherm as shown in **Figure 6**: Adsorption Isotherm variation with Temperature and their results are presented in **Table** 8: . It can be seen that with the increase in Temperature the working capacity of the sorbent (i.e. the amount of $C_2H_4$ adsorbable per unit weight of the sorbent) increases while the selectivity of $C_2H_4$ over $C_2H_6$ and $C_3H_6$ decreases as shown in **Table** 8: .

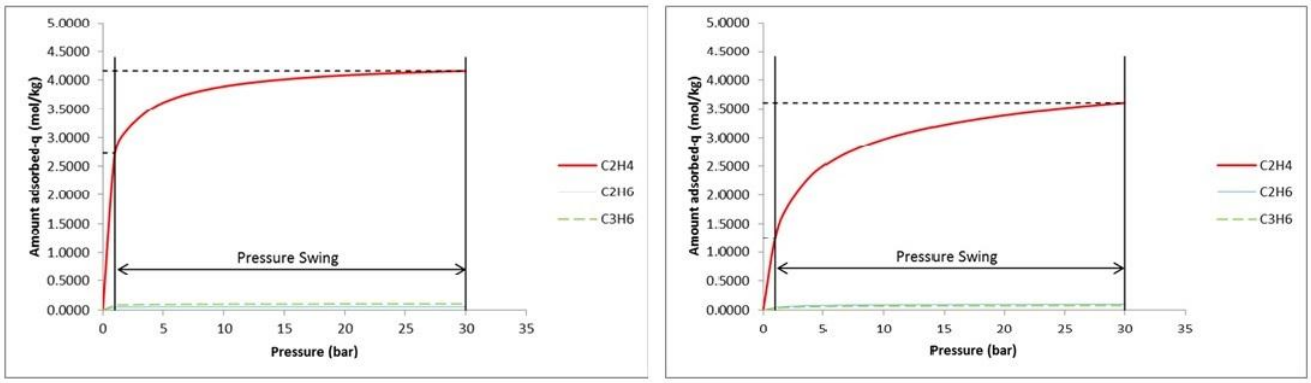


**Figure 6**: Adsorption Isotherm variation with Temperature

| Parameters | 80 °C | 150 °C |
|---|---|---|
| Working capacity (mol/kg) | 1.42 | 2.35 |
| Selectivity $C_2H_4/(C_2H_6\&C_3H_6)$ | 42 | 24 |

**Table** 8: Performance variation with Temperature

## 2.6 Equilibrium Model

An equilibrium based PSA model is developed using the above isotherm to approximately estimate the dimensions of the adsorption column and the corresponding amount of sorbent needed for complete adsorption of $C_2H_4$ from the feed stream shown in **Figure** 7. An assumption is made such that passing $C_2H_4$ rinse gas equivalent to the gas volume in the bed, makes the column completely saturated with $C_2H_4$. Also, the purity and recovery of $C_2H_4$ attainable through the equilibrium effects without involving the kinetic effects are studied and the results are presented in **Table** 9.

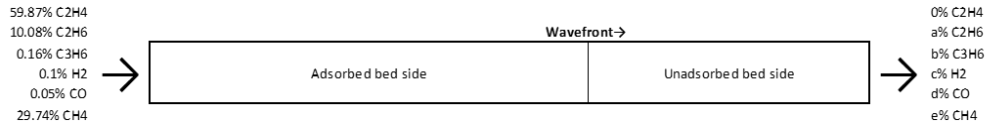


**Figure** 7: Equilibrium based PSA model for the stream after acetylene convertor

| Parameters | Value |
|---|---|
| Length of column | 7.8 m |
| Diameter of column | 2.5 m |
| Mass of adsorbent required | 28000 kg |
| Performance Parameters: | |
| Product Purity | 98.5 % |
| Product Recovery | 40 % |

**Table** 9: Results of Equilibrium based PSA model

## 2.7 Column model

Column model equations are summarised in **Table** 10.The intraparticle mass transfer resistance is described by a linear driving force, as discussed by Boon etal.(2014) and constitutive equations have been taken from the literature (Bird etal.,1960; Ruthven, 1984; Westerterpetal., 1987; Yang, 1987; Polingetal., 2001). Model parameters specific for the OPERA process are summarised in **Table** 11. The column dimensions obtained from the equilibrium model were taken as initial representative of OPERA columns and then varied for maximum adsorption capacity which matches with the industrial column dimensions **Fout! Verwijzingsbron niet gevonden.**.

| | | |
|---|---|---|
| Continuity | $\frac{\partial \rho}{\partial t} = -\frac{\partial \rho v}{\partial z} + \frac{1-\epsilon_b}{\epsilon_b} a_p \sum_i M_i N_i$ | A |
| Momentum | $0 = -\frac{\partial p}{\partial z} - f\frac{\rho \lvert u \rvert u}{d_p}$ | B |
| Mass balance | $\frac{\partial \rho \omega_i}{\partial t} = -\frac{\partial \rho v \omega_i}{\partial z} + \frac{\partial}{\partial z}\left(D_z \rho \frac{\partial \omega_i}{\partial z}\right) + \frac{1-\epsilon_b}{\epsilon_b} a_p M_i N_i$ | C |
| Equation of state | $p\, M = \rho\, R\, T$ | D |
| Intraparticle mass balance (linear driving force) | $N_i = \frac{\epsilon_p}{a_p} k_{LDF1,i}\left(\frac{\omega_i \rho}{M_i} - \langle c_i \rangle\right)$ | E |
| | $\frac{d\langle c_i \rangle}{dt} = k_{LDF1,i}\left(\frac{\omega_i \rho}{M_i} - \langle c_i \rangle\right) - \frac{\rho_p}{\epsilon_p}\frac{d\langle q_i \rangle}{dt}$ | F |
| Linear driving force mass transfer coefficient particle | $k_{LDF1,i} = \frac{15\, D_{p,i}}{\left(\frac{d_p}{2}\right)^2}$ | G |
| Macropore diffusivity | $D_{p,i} = \frac{\epsilon_p}{1.5\left(\frac{1}{D_m} + \frac{1}{D_k}\right)}$ | H |
| Molecular diffusivity | $D_m = 0.0018583\, \frac{\left(T^{\frac{3}{2}}\left(\sum_i \frac{1}{M_i}\right)^{\frac{1}{2}}\right)}{P\sigma^2\Omega}$ | I |
| Knudsen diffusivity | $D_k = 9.7\,.\,10^3\,.\,r_p\left(\frac{T}{M}\right)^{\frac{1}{2}}$ | J |
| Intracrystalline mass balance (linear driving force) | $\frac{\partial \langle q \rangle}{\partial t} = k_{LDF2,i}(q_i^* - \langle q_i \rangle)$ | K |

| | | |
|---|---|---|
| Linear driving force mass transfer coefficient crystal | $k_{LDF2,i} = \frac{15\ D_{c,i}}{\left(\frac{d_c}{2}\right)^2}$ | L |
| Micropore diffusivity | $D_{c,i} = D_{c0,i}\exp[-\frac{E_a}{R_g T}]$ | M |

**Table** 10: Column model equations

| Parameters | Value | |
|---|---|---|
| L | 10 | m |
| $d_c$ | 3 | m |
| $T_{wall}$ | 80 | C |
| $\epsilon_b$ | 0.32 | - |
| $\epsilon_p$ | 0.39 | - |
| $d_p$ | 2 x $10^{-3}$ | m |
| $\rho_p$ | 1072 | kg $m^{-3}$ |
| μ | 2 x $10^{-5}$ | $m^2$ $s^{-1}$ |
| $d_{crystal}$ | 2 x $10^{-6}$ | m |

**Table** 11: OPERA process parameters

## 2.8 Pressure Swing OPERA cycle

The OPERA cycle follows a number of steps that govern the performance of the process. The steps are schematically shown in **Figure** 8. for the OPERA cycle proposed in the current work aiming at a high purity $C_2H_4$ with the best possible recovery.

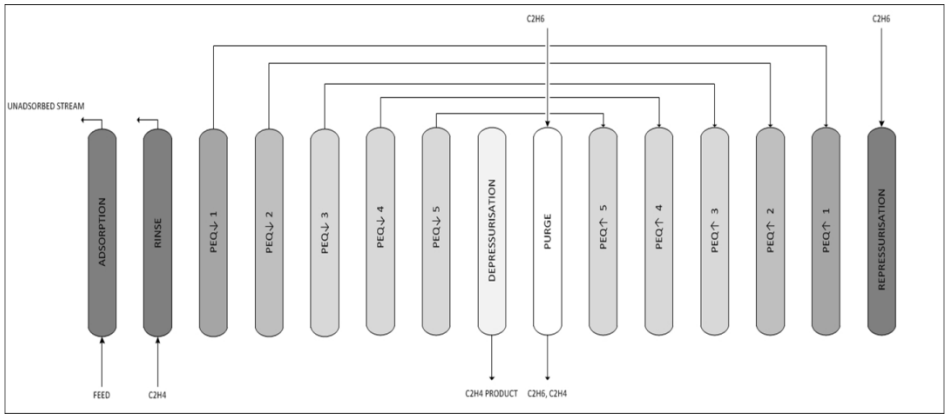


**Figure** 8: 15 step OPERA cycle

The single column model was extended to simulate consecutively all steps of a complete OPERA cycle for $C_2H_4$ separation.

The OPERA cycle consist of 15 steps:

1. Adsorption
2. Co-current rinse
3. Pressure equalisation 1
4. Pressure equalisation 2
5. Pressure equalisation 3
6. Pressure equalisation 4
7. Pressure equalisation 5
8. Depressurisation
9. Counter-current purge
10. Pressure equalisation 5
11. Pressure equalisation 4
12. Pressure equalisation 3
13. Pressure equalisation 2
14. Pressure equalisation 1
15. Repressurisation

During the adsorption step, $C_2H_4$ is adsorbed along with other components $C_2H_6$, $C_3H_6$ and some $CH_4$ remains in the gas volume.

Then a high pressure rinse is performed in which pure $C_2H_4$ stream is passed through the column. The use of rinse is known to improve the $C_2H_4$ purity **Fout! Verwijzingsbron niet gevonden.**.

After the rinse step, a number of pressure equalisation steps are carried out, in which a high pressure column is connected to a low pressure column in order to exchange gas from columns at higher pressures to columns in a lower pressure part of the cycle. This serves to remove the CH4 in the gas volume and also other impurities in the high pressure column by expanding the rinse gas and also to reduce the amount of gas fed to the column for repressurisation.

During the depressurisation step, relatively pure $C_2H_4$ product is collected.

In order to further desorb $C_2H_4$ from the column, a low pressure purge step follows.

Once sufficient $C_2H_4$ has been recovered, the column is repressurised with $C_2H_6$ or alternatively with feed stream.

Cycle timing for the 9 columns in parallel is as shown in **Table** 12 depicting the relative duration of each step. At every instant of time, there is at least one column in adsorption step thereby making the process to operate continuously.

| Duration | 1 | 2 | 3 | 4 | 5 | 6 | 7 | 8 | 9 | 10 | 11 | 12 | 13 | 14 | 15 | 16 | 17 | 18 |
|---|---|---|---|---|---|---|---|---|---|---|---|---|---|---|---|---|---|---|
| Column 1 | Adsorption | | | Rinse | | | PEQ↓1 | PEQ↓2 | PEQ↓3 | PEQ↓4 | PEQ↓5 | Blowdown | | Purge | PEQ↑5 | PEQ↑4 | PEQ↑3 | PEQ↑2 | PEQ↑1 | Repress |
| Column 2 | PEQ↑1 | Repress | Adsorption | | | Rinse | | PEQ↓1 | PEQ↓2 | PEQ↓3 | PEQ↓4 | PEQ↓5 | Blowdown | | Purge | PEQ↑5 | PEQ↑4 | PEQ↑3 | PEQ↑2 | |
| Column 3 | PEQ↑3 | PEQ↑2 | PEQ↑1 | Repress | Adsorption | | | Rinse | | PEQ↓1 | PEQ↓2 | PEQ↓3 | PEQ↓4 | PEQ↓5 | Blowdown | | Purge | PEQ↑5 | PEQ↑4 | |
| Column 4 | PEQ↑5 | PEQ↑4 | PEQ↑3 | PEQ↑2 | PEQ↑1 | Repress | Adsorption | | | Rinse | | PEQ↓1 | PEQ↓2 | PEQ↓3 | PEQ↓4 | PEQ↓5 | Blowdown | | Purge | |
| Column 5 | Blowdown | Purge | PEQ↑5 | PEQ↑4 | PEQ↑3 | PEQ↑2 | PEQ↑1 | Repress | Adsorption | | Rinse | | PEQ↓1 | PEQ↓2 | PEQ↓3 | PEQ↓4 | PEQ↓5 | Blowdown | | |
| Column 6 | PEQ↓5 | Blowdown | | Purge | PEQ↑5 | PEQ↑4 | PEQ↑3 | PEQ↑2 | PEQ↑1 | Repress | Adsorption | | Rinse | | PEQ↓1 | PEQ↓2 | PEQ↓3 | PEQ↓4 | | |
| Column 7 | PEQ↓3 | PEQ↓4 | PEQ↓5 | Blowdown | | Purge | PEQ↑5 | PEQ↑4 | PEQ↑3 | PEQ↑2 | PEQ↑1 | Repress | Adsorption | | Rinse | | PEQ↓1 | PEQ↓2 | | |
| Column 8 | PEQ↓1 | PEQ↓2 | PEQ↓3 | PEQ↓4 | PEQ↓5 | Blowdown | | Purge | PEQ↑5 | PEQ↑4 | PEQ↑3 | PEQ↑2 | PEQ↑1 | Repress | Adsorption | | Rinse | | | |
| Column 9 | Rinse | | PEQ↓1 | PEQ↓2 | PEQ↓3 | PEQ↓4 | PEQ↓5 | Blowdown | | Purge | PEQ↑5 | PEQ↑4 | PEQ↑3 | PEQ↑2 | PEQ↑1 | Repress | Adsorption | | | |

**Table** 12: 9 columns for 11-step SEWGS cycle with co-current C2H4 rinse and counter-current C2H6 purge

Numerically, a single column is simulated in time while the connecting steps are stored. Timing is controlled by varying the total cycle time and dividing it over the steps as indicated by the relative duration in **Table** 12. The simulation continues for a number of cycles until cyclic steady state is reached. Typically 20-30 cycles are required for the OPERA process to reach cyclic steady state. In order to save time, the column is coarsely divided into 80 finite differences, but it was verified that a more refined grid of 200 points yielded almost the same results as seen in **Figure** 9.

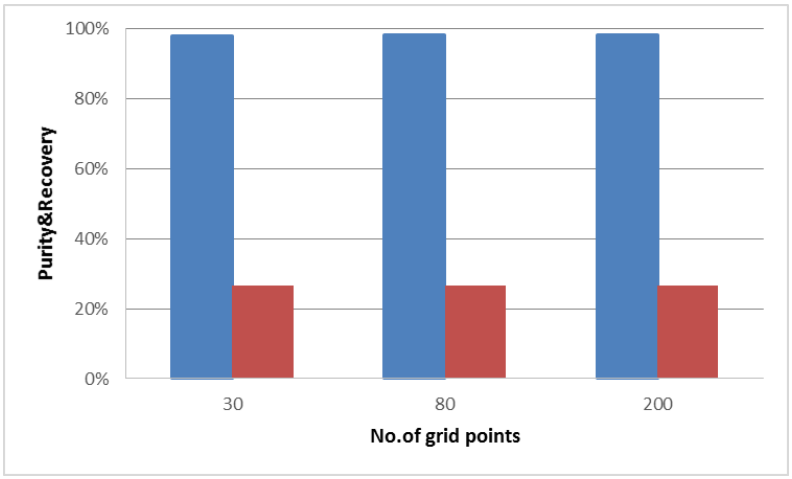


**Figure** 9: Effect of grid points on bed performance

The simulation is run with the standard parameters detailed in **Table** 11 and **Table** 13.

For the overall OPERA cycle, the design criteria are generally formulated in terms of the purity of $C_2H_4$ product and the amount of $C_2H_4$ product recovered divided by the amount of $C_2H_4$ fed. The former is important because any $C_2H_6$, $C_3H_6$ and $CH_4$ that end up in the $C_2H_4$ product will reduce the quality of the product. The later quantifies the amount of $C_2H_4$ that can be captured from the feed. The performance of the cycle within these design criteria can be expressed in three dependent variables:

(1) Purity, weight percentage of $C_2H_4$ in the product stream
(2) Recovery, amount of $C_2H_4$ recovered from the feed stream
(3) Productivity, the amount of $C_2H_4$ produced per unit time per amount of sorbent

The optimal OPERA cycle would consequently minimise capital cost (CAPEX) and operating cost (OPEX), by optimisation of the total $C_2H_4$ consumption and productivity.

| Steps | Unit | Value |
|---|---|---|
| **Feed** | | |
| Relative duration | - | 2/18 |
| $F_m$ | $kgs^{-1}$ | 15 |
| $P_{out}$ | bar | 29.8 |
| $\omega_{H2}$ | - | 0.001 |
| $\omega_{CO}$ | - | 0.0005 |
| $\omega_{CH4}$ | - | 0.2974 |
| $\omega_{C2H4}$ | - | 0.5987 |
| $\omega_{C2H6}$ | - | 0.1008 |
| $\omega_{C3H6}$ | - | 0.0016 |
| **Rinse** | | |
| Relative duration | - | 2/18 |
| $F_m$ | $kgs^{-1}$ | Varied |
| $P_{out}$ | bar | 29.8 |
| $\omega_{C2H4}$ | - | 1 |
| **Pressure equalisation 1-5** | | |
| Relative duration | - | 1/18 |
| $P_{out}$ | bar | Interpolated |
| **Depressurisation** | | |
| Relative duration | - | 2/18 |
| $p_{out}$ | bar | 1 |
| **Purge** | | |
| Relative duration | - | 1/18 |
| $F_m$ | $kgs^{-1}$ | Varied |
| $P_{out}$ | bar | 1 |
| $\omega_{C2H6}$ | - | 1 |
| **Pressure equalisation 5-1** | | |
| Relative duration | - | 1/18 |
| $F_m$ | $kgs^{-1}$ | From providing steps |
| **Repressurisation** | | |
| Relative duration | - | 1/18 |
| $F_m$ | $kgs^{-1}$ | Interpolated |

**Table** 13: OPERA boundary conditions for a single train of 9 columns

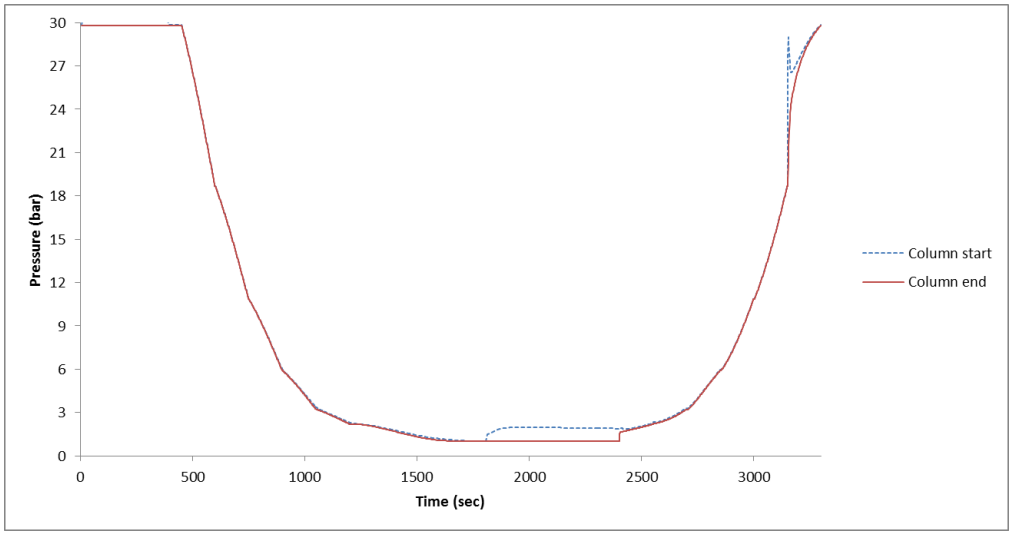


**Figure** 10: Column pressure development over the 15 step OPERA cycle

Pressure variation with time along the OPERA cycle is described in **Figure** 10. Pressure at start of the column and at the end of the column are plotted in the figure. From the graph, it is observed that the pressure drop along the column is not high. But it can be seen that during Repressurisation step, at the start of the column a shock occurs due to the high inlet mass flow rate.

# 3

# Results & Discussion

A parameter study was done in order to evaluate the performance of the OPERA cycle under different operating conditions. Aiming at 99.9% $C_2H_4$ purity and 40% $C_2H_4$ recovery, simulations are run for varied rinse, purge, particle size, number of pressure equalisations, pressure equalisation time, blowdown time, temperature, and position. Each of the condition yields a cyclic steady state with $C_2H_4$ purity and recovery values.

## 3.1 Rinse variation

The rinse step in PSA is an adsorption step in which the concentration of $C_2H_4$ in the column is increased by passing pure $C_2H_4$ stream at high pressure. Generally, a fraction of the $C_2H_4$ product is used to rinse the bed. The amount of rinse required affects the product purity as well as its recovery. As the amount of rinse increases, rinsing becomes more effective providing a bed with high $C_2H_4$ loading and leading to an increased product purity. In principal, the bed should be fully loaded with $C_2H_4$, thus more rinsing is necessary. At the same time, since rinsing is done using the pure ethylene product, increase in the rinse amount decreases the product recovery. Generally, the rinse amount specification for PSA is given by the rinse-to-product amount ratio.

Simulations were run with different values of rinse-to-product amount ratio. The results are presented in **Figure** 11 showing the effect of this ratio on product purity and recovery. It can be seen that as this ratio increases, the product purity increases as well, but the recovery decreases. The rate of increase in purity is much slower than the rate of decrease in recovery. From, these results we can observe that the rinse-to-product amount ratio should never be greater than 1. In fact, if the ratio is over 0.5, the compression energy for rinse gas becomes very high, thereby making the process energy intensive which is undesirable.

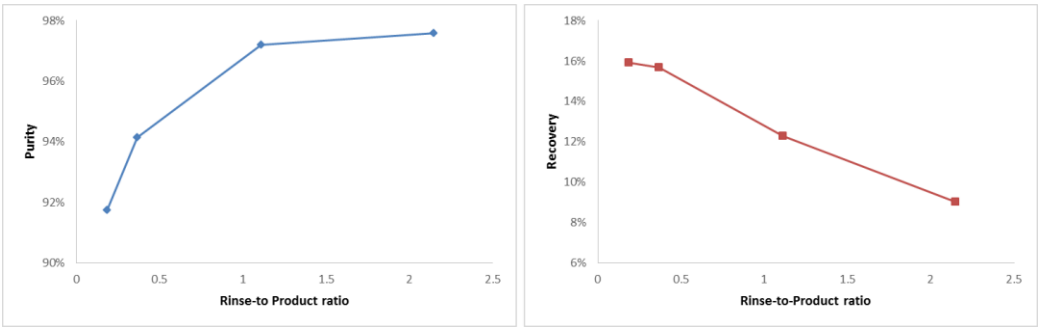


(a) (b)

**Figure** 11: Effect of rinse-to-product ratio on bed performance (a) Product purity. (b) Product recovery

| Rinse (kg) | $P_H$ (bar) | $P_L$ (bar) | Time (sec) | | | | | | $f_{Ads}$ (kg/s) | $f_{Rinse}$ (kg/s) | $f_{Purge}$ (kg/s) | $f_{Repress}$ (kg/s) |
|---|---|---|---|---|---|---|---|---|---|---|---|---|
| | | | Ads | Rinse | PEQ | BD | Purge | Repress | | | | |
| 100 | 30 | 1 | 360 | 25 | 90 | 90 | 1200 | 150 | 15 | 4 | 4 | 200 |
| 200 | 30 | 1 | 360 | 50 | 90 | 90 | 1200 | 150 | 15 | 4 | 4 | 200 |
| 600 | 30 | 1 | 360 | 150 | 90 | 90 | 1200 | 150 | 15 | 4 | 4 | 200 |
| 800 | 30 | 1 | 360 | 200 | 90 | 90 | 1200 | 150 | 15 | 4 | 4 | 200 |

**Table** 14: Simulation conditions for the study on rinse variation

## 3.2 Purge variation

The purge step in PSA is a desorption step in which the adsorbents are regenerated by desorbing the adsorbed $C_2H_4$ component. The amount of purge used affects the product purity as well as its recovery. As the amount of purge increases, purging becomes more effective providing a regenerated bed with adsorbents of less $C_2H_4$ loading and leading to an increased product purity.

Simulations were run with different values of $C_2H_6$ purge amount. The results are presented in **Figure** 12 showing the effect of purge amount on product purity and recovery. It can be seen that as the purge amount increases, the product purity increases as well, but the recovery decreases. The rate of increase in purity is much slower than the rate of decrease in recovery. From, these results we can observe that the purge amount should neither be too low nor be higher than the amount of $C_2H_6$ available in the feed.

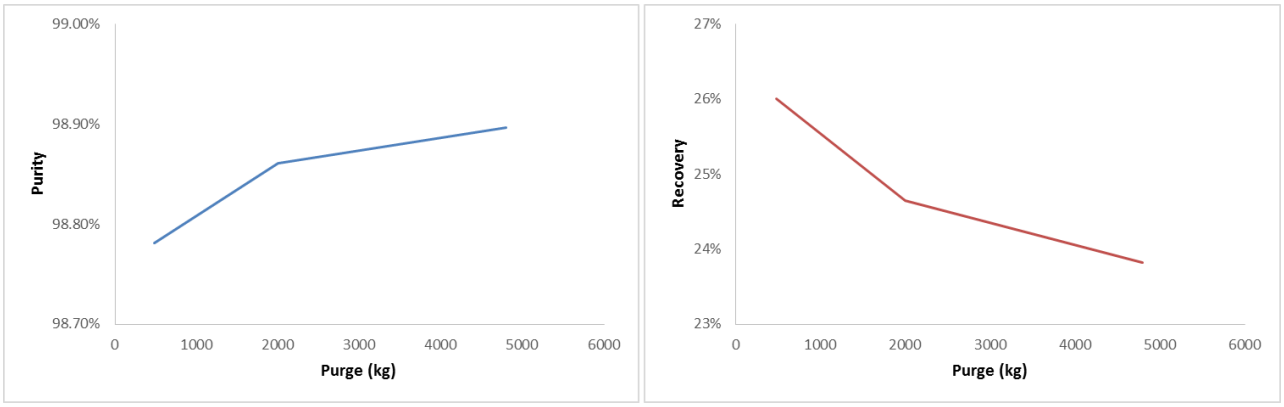


(a) (b)

**Figure** 12: Effect of Purge amount on bed performance (a) Product purity. (b) Product recovery

| Purge (kg) | $P_H$ (bar) | $P_L$ (bar) | Time (sec) | | | | | | $f_{Ads}$ (kg/s) | $f_{Rinse}$ (kg/s) | $f_{Purge}$ (kg/s) | $f_{Repress}$ (kg/s) |
|---|---|---|---|---|---|---|---|---|---|---|---|---|
| | | | Ads | Rinse | PEQ | BD | Purge | Repress | | | | |
| 480 | 30 | 1 | 360 | 150 | 60 | 300 | 120 | 150 | 15 | 3.5 | 4 | 200 |
| 2000 | 30 | 1 | 360 | 150 | 60 | 300 | 500 | 150 | 15 | 3.5 | 4 | 200 |
| 4800 | 30 | 1 | 360 | 150 | 60 | 300 | 1200 | 150 | 15 | 3.5 | 4 | 200 |

**Table** 15: Simulation conditions for the study on purge variation

## 3.3 Particle size variation

Particle size affects the bed performance in two ways. If other parameters remain constant, a lower particle size leads to higher bed pressure drop as shown in **Figure 14**. On the other hand, a lower particle size means a higher surface area of the adsorbent and hence a higher mass transfer rate. Both of these properties increase the product recovery.

Thus, there are two opposite effects of particle size: high product purity requires small particle size and a low pressure drop is achieved with large particle size.

Simulation studies were run with various particle sizes and their results are shown in Fig. 11. The effect of particle size on product purity is significant for both bulk separation and purification processes. **Figure** 13 shows that higher particle size decreases both the product purity and recovery.

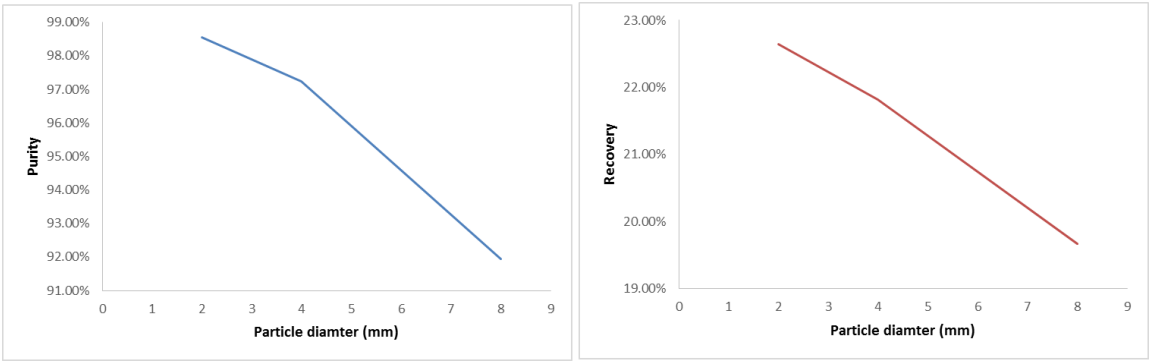


(a) (b)

**Figure** 13: Effect of Particle size on bed performance (a) Product purity. (b) Product recovery

| $d_p$ (mm) | $P_H$ (bar) | $P_L$ (bar) | Time (sec) | | | | | | $f_{Ads}$ (kg/s) | $f_{Rinse}$ (kg/s) | $f_{Purge}$ (kg/s) | $f_{Repress}$ (kg/s) |
|---|---|---|---|---|---|---|---|---|---|---|---|---|
| | | | Ads | Rinse | PEQ | BD | Purge | Repress | | | | |
| 2 | 30 | 1 | 360 | 150 | 60 | 300 | 1200 | 150 | 15 | 3.5 | 4 | 200 |
| 4 | 30 | 1 | 360 | 150 | 60 | 300 | 1200 | 150 | 15 | 3.5 | 4 | 200 |
| 8 | 30 | 1 | 360 | 150 | 60 | 300 | 1200 | 150 | 15 | 3.5 | 4 | 200 |

**Table** 16: Simulation conditions for the study on particle size variation

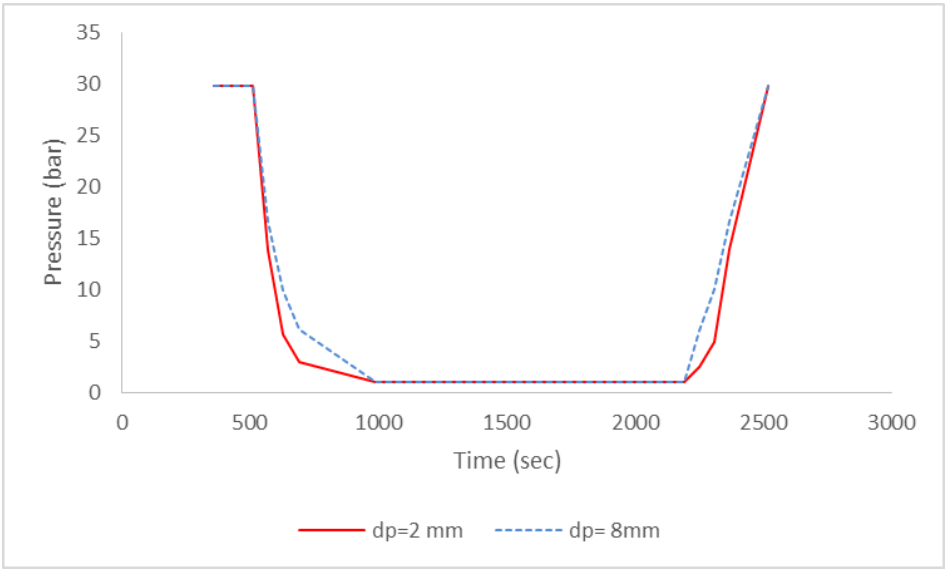


**Figure 14**: Pressure variation along the cycle with varied particle size

## 3.4 Number of Pressure Equalisations variation

After a bed has been purged and another bed has completed its high pressure rinse step, instead of blowing down the second bed directly, the two beds can be connected to each other through their product ends in order to equalise their pressures. Thus the first bed is partially pressurised with gas from the outlet of the second bed. After the pressure equalisations, the two beds are disconnected and the first bed is further repressurised with $C_2H_6$/feed gas while the second bed is vented to complete the blowdown. The pressure equalisation step conserves energy because the low pressure bed is partially pressurised with the compressed gas from the high pressure bed. Also, the impurities in the bed mainly the $CH_4$ in the gas volume are pushed out of the high pressure bed, making the column highly saturated with $C_2H_4$ and thereby having high purity $C_2H_4$ product during the blowdown step. But with increase in the number of pressure equalisations, the pressure drop available for blowdown step decreases, thereby affecting the product recovery. Also with increase in the number of pressure equalisations, the number of connecting columns that are needed for the pressure equalisation also increases, thereby increasing the capital cost. Based on these considerations, pressure equalisation steps are incorporated in the PSA process.

Simulations were run with different number of pressure equalisations and their results are presented in **Figure 15**. It can be seen that the increase in the number of pressure equalisations favours product purity as the $C_2H_4$ concentration in the bed increases. But the product recovery decreases as along with the impurities, some $C_2H_4$ is also pushed out of the high pressure column during the pressure drop.

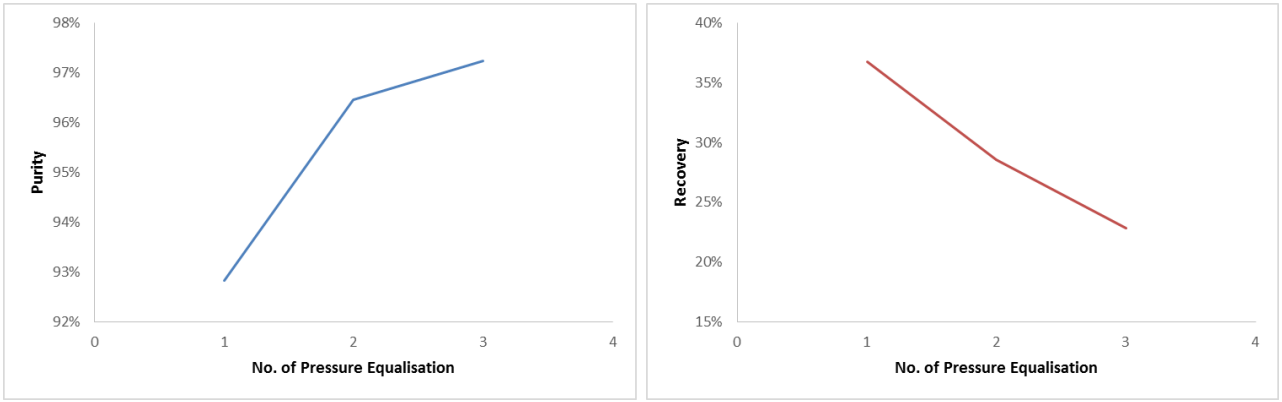


(a) (b)

**Figure 15**: : Effect of Number of Pressure Equalisations on bed performance (a) Product purity. (b) Product recovery

| PEQ No. | $P_H$ (bar) | $P_L$ (bar) | Time (sec) | | | | | | $f_{Ads}$ (kg/s) | $f_{Rinse}$ (kg/s) | $f_{Purge}$ (kg/s) | $f_{Repress}$ (kg/s) |
|---|---|---|---|---|---|---|---|---|---|---|---|---|
| | | | Ads | Rinse | PEQ | BD | Purge | Repress | | | | |
| 1 | 30 | 1 | 360 | 150 | 60 | 300 | 1200 | 150 | 15 | 3.5 | 4 | 200 |
| 2 | 30 | 1 | 360 | 150 | 60 | 300 | 1200 | 150 | 15 | 3.5 | 4 | 200 |
| 3 | 30 | 1 | 360 | 150 | 60 | 300 | 1200 | 150 | 15 | 3.5 | 4 | 200 |

**Table** 17: Simulation conditions for the study on number of pressure equalisations variation

## 3.5 Pressure Equalisation Time variation

Similar to the number of pressure equalisations variation, simulations were run with different pressure equalisation time and their results are presented in **Figure 16**. It can be seen from **Figure** 17 that the increase in the pressure equalisation time favours product purity as the $C_2H_4$ concentration in the bed increases by removal of impurities mainly $CH_4$ in the gas volume. But the product recovery decreases as some $C_2H_4$ is also pushed out of the high pressure column along with the impurities during the pressure drop. So, the choice of the pressure equalisation time depends on whether a high purity product is needed or if high recovery is important than purity.

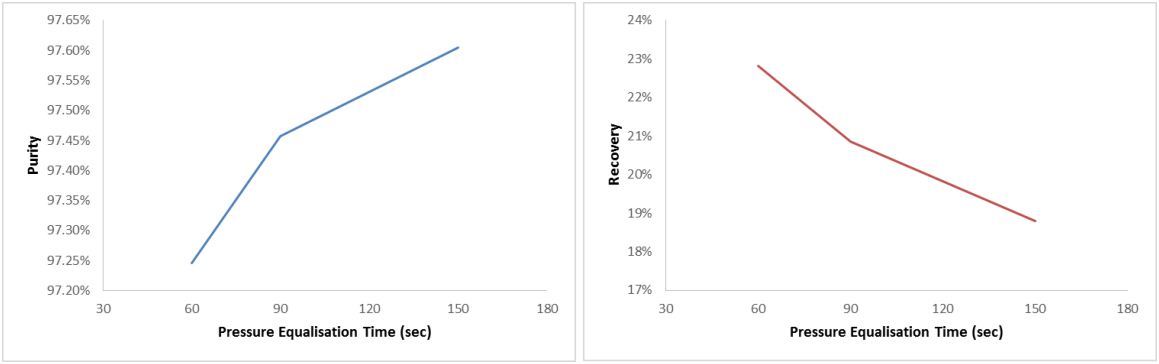


(a) (b)

**Figure 16**: : Effect of Pressure Equalisation time on bed performance (a) Product purity. (b) Product recovery

| $P_H$ (bar) | $P_L$ (bar) | Time (sec) | | | | | | $f_{Ads}$ (kg/s) | $f_{Rinse}$ (kg/s) | $f_{Purge}$ (kg/s) | $f_{Repress}$ (kg/s) |
|---|---|---|---|---|---|---|---|---|---|---|---|
| | | Ads | Rinse | PEQ | BD | Purge | Repress | | | | |
| 30 | 1 | 360 | 150 | 60 | 300 | 1200 | 150 | 15 | 3.5 | 4 | 200 |
| 30 | 1 | 360 | 150 | 90 | 300 | 1200 | 150 | 15 | 3.5 | 4 | 200 |
| 30 | 1 | 360 | 150 | 150 | 300 | 1200 | 150 | 15 | 3.5 | 4 | 200 |

**Table** 18: Simulation conditions for the study on pressure equalisation time variation

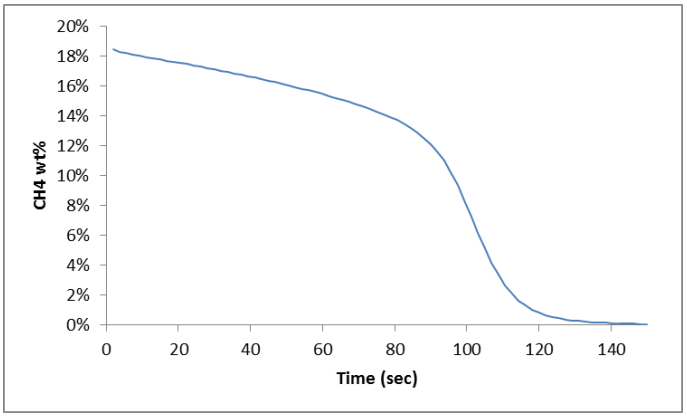


**Figure** 17: Effect of Pressure Equalisation time on $CH_4$ % in the bed

## 3.6 Blowdown Time variation

During the blowdown step, the high purity product is desorbed from the bed by reducing the pressure. **Figure** 18 shows the simulation results corresponding to different time allocations to the blowdown step. It can be seen that the increase in blowdown time increases recovery as well as the purity of the product. As the blowdown time increases, more $C_2H_4$ is blown down from the bed thereby increasing the recovery but after a point of time, saturation occurs thereby the desorption stops. At the same time, the purity increases, as after a while even higher purity $C_2H_4$ will be desorbed from the bed. **Figure** 19 shows the pressure profile along the blowdown step at the start and end positions of the column for a 5 pressure equalisation cycle.

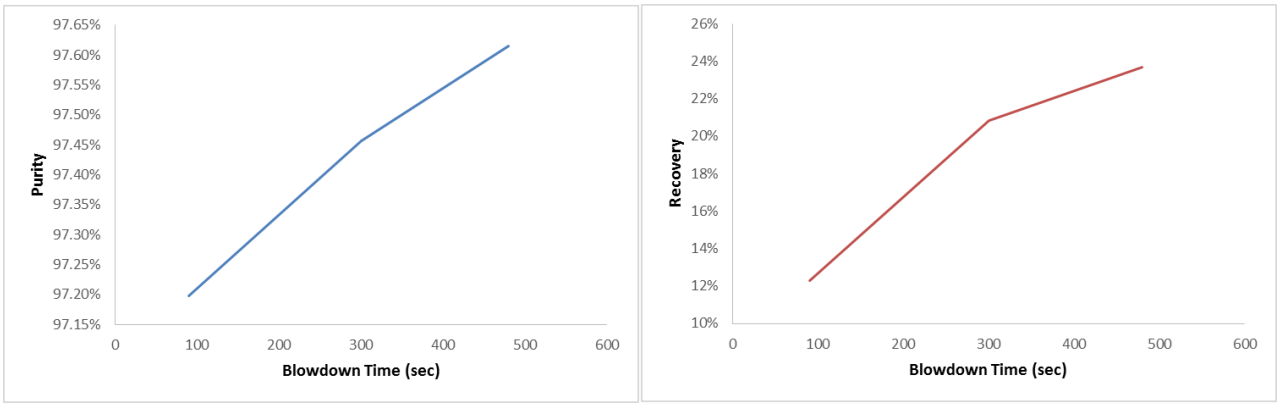


(a) (b)

**Figure** 18: Effect of Blowdown time on bed performance (a) Product purity. (b) Product recovery

| $P_H$ (bar) | $P_L$ (bar) | Time (sec) | | | | | | $f_{Ads}$ (kg/s) | $f_{Rinse}$ (kg/s) | $f_{Purge}$ (kg/s) | $f_{Repress}$ (kg/s) |
|---|---|---|---|---|---|---|---|---|---|---|---|
| | | Ads | Rinse | PEQ | BD | Purge | Repress | | | | |
| 30 | 1 | 360 | 150 | 90 | 90 | 1200 | 150 | 15 | 3.5 | 4 | 200 |
| 30 | 1 | 360 | 150 | 90 | 300 | 1200 | 150 | 15 | 3.5 | 4 | 200 |
| 30 | 1 | 360 | 150 | 90 | 480 | 1200 | 150 | 15 | 3.5 | 4 | 200 |

**Table** 19: Simulation conditions for the study on blowdown time variation

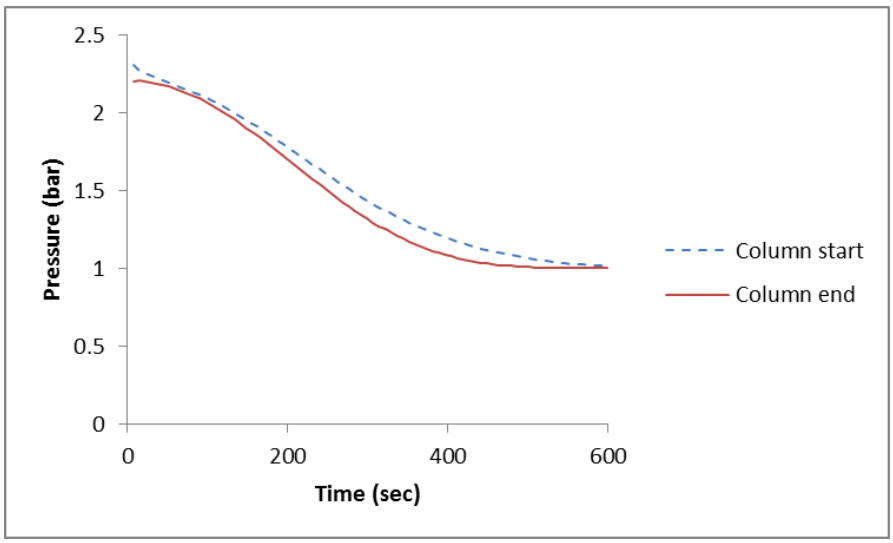


**Figure** 19: Pressure drop profile at the start and end of the column during the blowdown step

## 3.7 Number of Grid Points variation

Simulations were run with different grid points and their results are presented in **Figure** 20. It can be observed that both product purity and recovery are sensitive to the number of grid points which appears to be related to the role of relatively sharp concentration profiles. Between 80 and 200 grid points, no significant difference exist (<0.1%) and the former was chosen to perform the cycle simulations presented here.

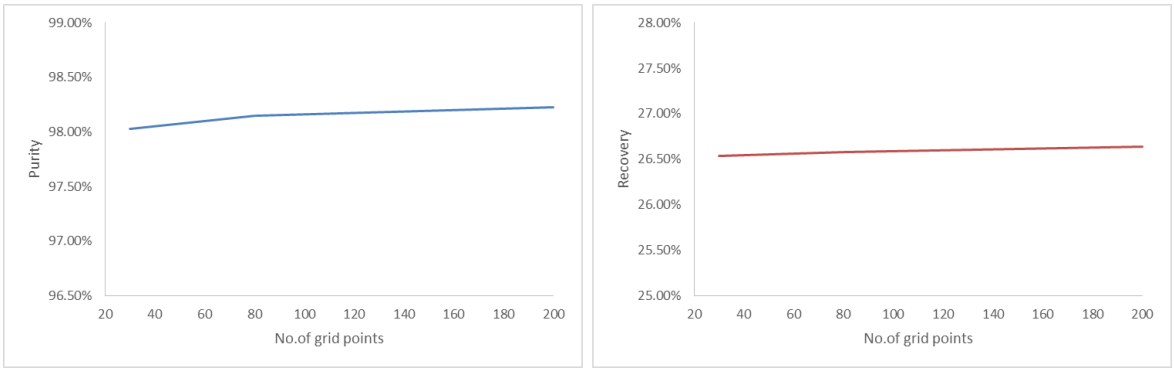


(a) (b)

**Figure** 20: Effect of Grid points on bed performance (a) Product purity. (b) Product recovery

| Grid points | $P_H$ (bar) | $P_L$ (bar) | Time (sec) | | | | | | $f_{Ads}$ (kg/s) | $f_{Rinse}$ (kg/s) | $f_{Purge}$ (kg/s) | $f_{Repress}$ (kg/s) |
|---|---|---|---|---|---|---|---|---|---|---|---|---|
| | | | Ads | Rinse | PEQ | BD | Purge | Repress | | | | |
| 30 | 30 | 1 | 390 | 60 | 150 | 600 | 900 | 150 | 15 | 4 | 4 | 70 |
| 80 | 30 | 1 | 390 | 60 | 150 | 600 | 900 | 150 | 15 | 4 | 4 | 70 |
| 200 | 30 | 1 | 390 | 60 | 150 | 600 | 900 | 150 | 15 | 4 | 4 | 70 |

**Table** 20: Simulation conditions for the study on grid points variation

## 3.8 Temperature variation

As the operating temperature increases, the amount of gas adsorbed on the adsorbent will increase. Hence the recovery of the product increase. But, along with the desired product $C_2H_4$, other components are also adsorbed more thereby decreasing the product purity as seen from **Table** 8: Performance variation with Temperature. Simulations were run with different operating temperature and their results are presented in **Figure** 21.

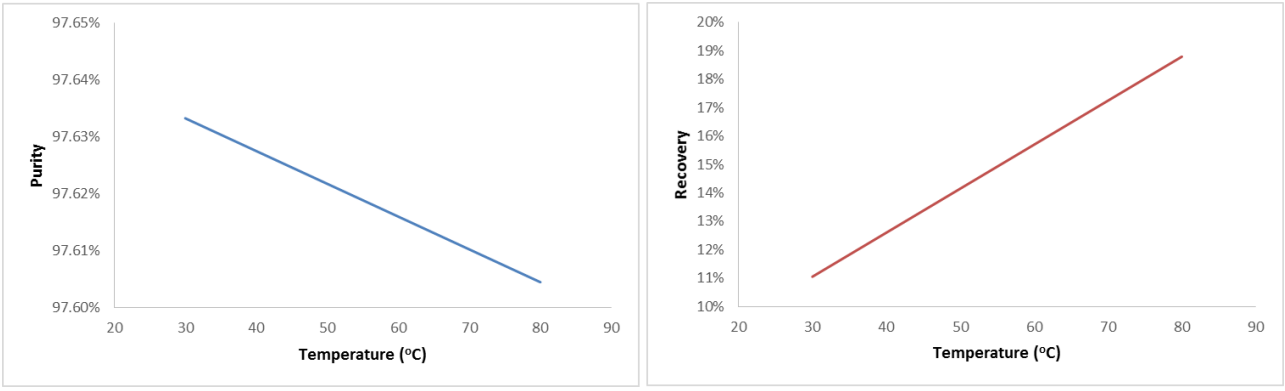


(a) (b)

**Figure** 21: Effect of temperature variation on bed performance (a) Product purity. (b) Product recovery

| T (°C) | $P_H$ (bar) | $P_L$ (bar) | Time (sec) | | | | | | $f_{Ads}$ (kg/s) | $f_{Rinse}$ (kg/s) | $f_{Purge}$ (kg/s) | $f_{Repress}$ (kg/s) |
|---|---|---|---|---|---|---|---|---|---|---|---|---|
| | | | Ads | Rinse | PEQ | BD | Purge | Repress | | | | |
| 30 | 30 | 1 | 390 | 60 | 150 | 300 | 1200 | 150 | 15 | 4 | 4 | 70 |
| 80 | 30 | 1 | 390 | 60 | 150 | 300 | 1200 | 150 | 15 | 4 | 4 | 70 |

**Table** 21: Simulation conditions for the study on temperature variation

## 3.9 Position variation

Simulations were run with varying the position of the OPERA system in the Naphtha cracking process and their results are presented in **Figure** 22. It can be seen that for the OPERA system before the $C_2$ splitter, due to the low temperature, the product recovery is very low although the purity is higher. For the same system after the $C_2H_2$ convertor, due to high temperature, the product recovery is much higher although the purity of the product is comparatively lower. Thereby supporting the decision of OPERA system positioning after $C_2H_2$ convertor.

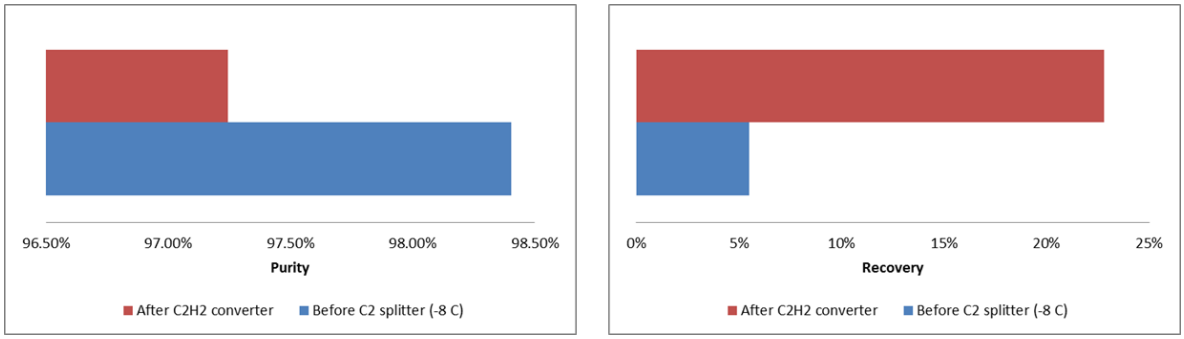


(a) (b)

**Figure** 22: Effect of Positioning on bed performance (a) Product purity. (b) Product recovery

| Position | T (°C) | $P_H$ (bar) | $P_L$ (bar) | Time (sec) | | | | | | $f_{Ads}$ (kg/s) | $f_{Rinse}$ (kg/s) | $f_{Purge}$ (kg/s) | $f_{Repress}$ (kg/s) |
|---|---|---|---|---|---|---|---|---|---|---|---|---|---|
| | | | | Ads | Rinse | PEQ | BD | Purge | Repress | | | | |
| After C2H2 convertor | 80 | 30 | 1 | 360 | 150 | 60 | 300 | 1200 | 150 | 15 | 3.5 | 4 | 70 |
| Before C2 splitter | -8 | 25 | 1 | 360 | 150 | 60 | 300 | 1200 | 150 | 15 | 3.5 | 4 | 70 |

**Table** 22: Simulation conditions for the study on positioning variation

The effect of various factors on the performance parameters i.e. purity and recovery of $C_2H_4$ has been studied from the previous section. Considering the effects, an optimised cycle with five pressure equalisations is designed to achieve high purity (>99.5 wt.%) and maximum possible recovery for that purity. Simulations are run to achieve the Cyclic Steady State condition and their results are presented below.

| T (°C) | $P_H$ (bar) | $P_L$ (bar) | Time (sec) | | | | | | $f_{Ads}$ (kg/s) | $f_{Rinse}$ (kg/s) | $f_{Purge}$ (kg/s) | $f_{Repress}$ (kg/s) |
|---|---|---|---|---|---|---|---|---|---|---|---|---|
| | | | Ads | Rinse | PEQ | BD | Purge | Repress | | | | |
| 80 | 30 | 1 | 390 | 60 | 150 | 600 | 600 | 150 | 15 | 4 | 4 | 70 |

**Table** 23: Optimised OPERA cycle conditions

Variation of gas phase concentration profile at the outlet of the column as a function of time is presented in **Figure** 24. It can be observed from **Figure** 24 (1) that during adsorption step after 390 seconds, the outlet gas concentration profile becomes steady representing that the bed is saturated and it is not possible to adsorb anymore $C_2H_4$. Hence, the adsorption step is stopped at 390 seconds to prevent further loss of $C_2H_4$. **Figure** 24(3) (4) (5) (6) and (7) shows the outlet concentration profiles of the pressure equalisation steps of the high pressure columns and **Figure** 24 (10) (11) (12) (13) (14) and (15) shows that of the low pressure columns. It can be seen that there is an exchange of gases from the high pressure columns to the low pressure columns. Gas phase concentration profile along the bed at the end of each step is shown in Figure 18. At the end of fifth pressure equalisation, the bed is filled with pure $C_2H_4$ as can be seen from **Figure** 23 (7). The column is now ready for the blowdown step in which pure $C_2H_4$ is desorbed from the bed as shown in **Figure** 24(8). After the blowdown step, in order to regenerate the bed free of $C_2H_4$, a purge step is performed using $C_2H_6$ in which the remaining $C_2H_4$ in the bed is removed as shown in **Figure** 24(9). After the low pressure equalisation steps, the bed is repressurised to 30 bar in order to make it ready for the next cycle adsorption step as shown in **Figure** 23 (15).

The loading of different gases on the Zeolite 13X adsorbent at the end of each step is shown in **Figure** 25. It can be seen from **Figure** 25 (1) that the adsorption capacity for $C_2H_4$ is much higher compared to that of $C_2H_6$ and $C_3H_6$ which is a positive scenario for $C_2H_4$ adsorption.
But after the blowdown step, it can be seen from **Figure** 25 (8) that the adsorbent is largely filled with $C_2H_4$ as more $C_2H_4$ is retained in the bed due to its strong interaction with Zeolite 13X sorbent molecules. Even after purging the column with $C_2H_6$, it can be observed from **Figure** 25 (9) that still more $C_2H_4$ is retained in the bed. This is a negative scenario as the recovery decreases.

Also, It can be seen from **Table** 24 that the maximum purity attainable is <99.9% . Over a period of cycle before reaching the cyclic steady state condition, the weight percentage of $C_3H_6$ in the product $C_2H_4$ stream decreases steadily which is a possible scenario. But the weight percentage of $C_2H_6$ decreases initially but later starts to increase. This is a negative scenario as the purity of $C_2H_4$ product is limited by $C_2H_6$.

| | |
|---|---|
| Purity | 99.7 wt.% |
| Recovery | 17 wt.% |
| Rinse-to-Product ratio (mass basis) | 0.35 |
| Purge-to Product ratio (mass basis) | 3.5 |

**Table** 24: Cyclic Steady State result for optimised OPERA cycle

From the above results, we can clearly see that a sorbent with higher selectivity of $C_2H_4$ over $C_2H_6$ is needed to achieve a purity greater than 99.9 wt%.

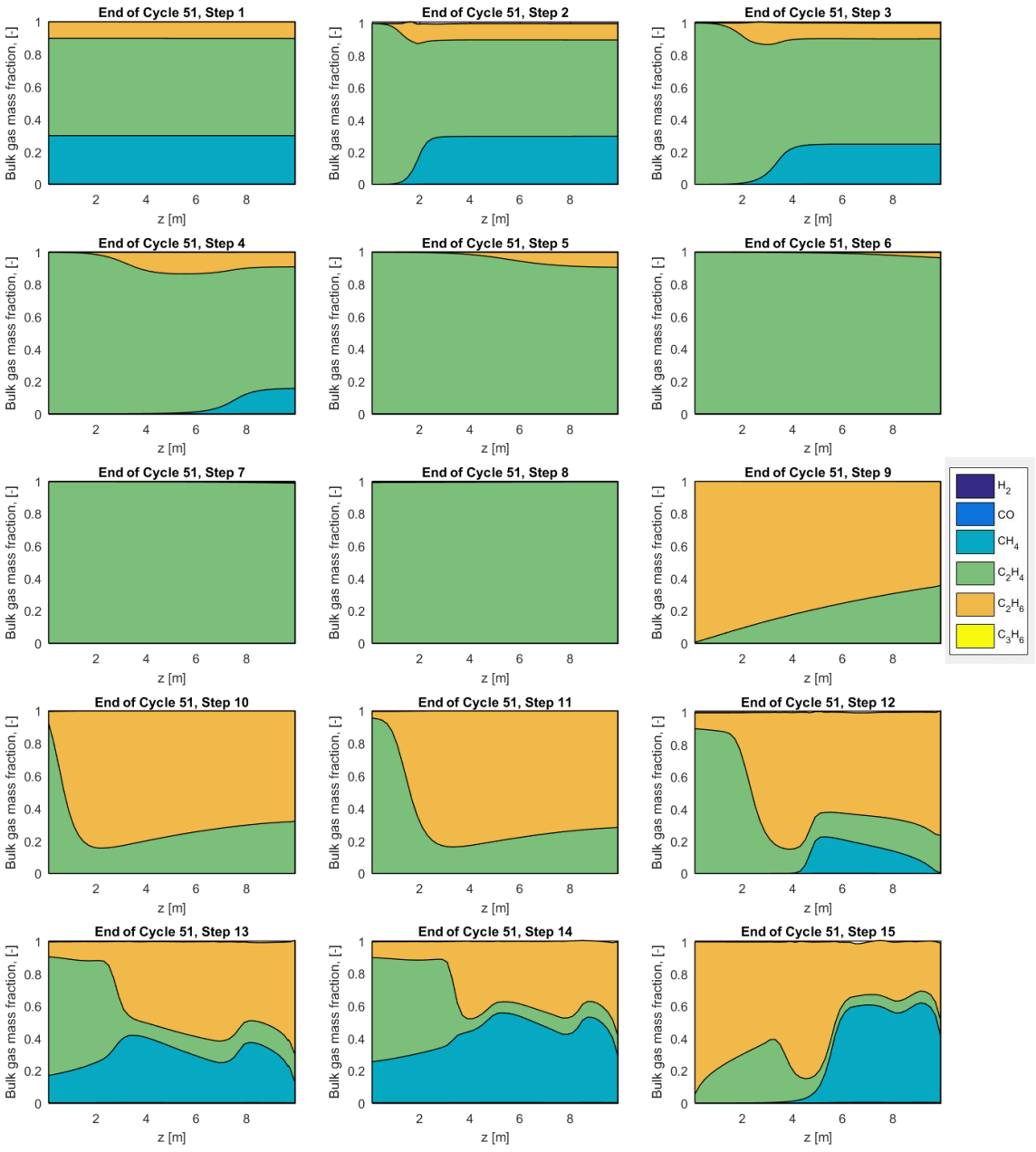


**Figure** 23: Gas phase concentrations vs axial coordinate at the end of each step during OPERA cycle, conditions in **Table** 23 (1) Adsorption (2) Rinse (3) Pressure equalisation 1 (4) Pressure equalisation 2 (5) Pressure equalisation 3 (6) Pressure equalisation 4 (7) Pressure equalisation 5 (8) Depressurisation (9) Purge (10) Pressure equalisation 5 (11) Pressure equalisation 4 (12) Pressure equalisation 3 (13) Pressure equalisation 2 (14) Pressure equalisation 1 (15) Repressurisation

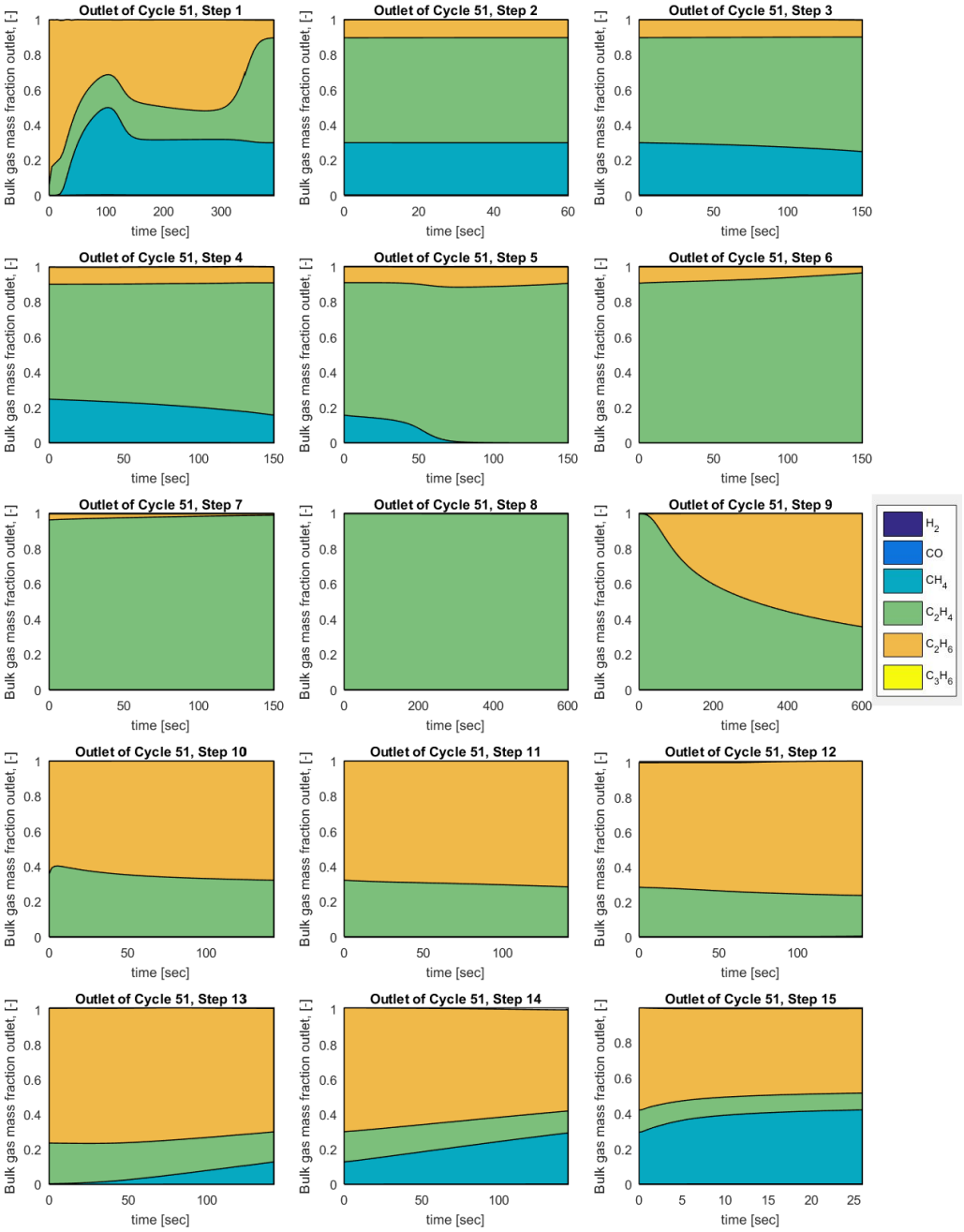


**Figure** 24: Outlet gas phase concentration vs time variation for each step of OPERA cycle, conditions in **Table** 23 (1) Adsorption (2) Rinse (3) Pressure equalisation 1 (4) Pressure equalisation 2 (5) Pressure equalisation 3 (6) Pressure equalisation 4 (7) Pressure equalisation 5 (8) Depressurisation (9) Purge (10) Pressure equalisation 5 (11) Pressure equalisation 4 (12) Pressure equalisation 3 (13) Pressure equalisation 2 (14) Pressure equalisation 1 (15) Repressurisation

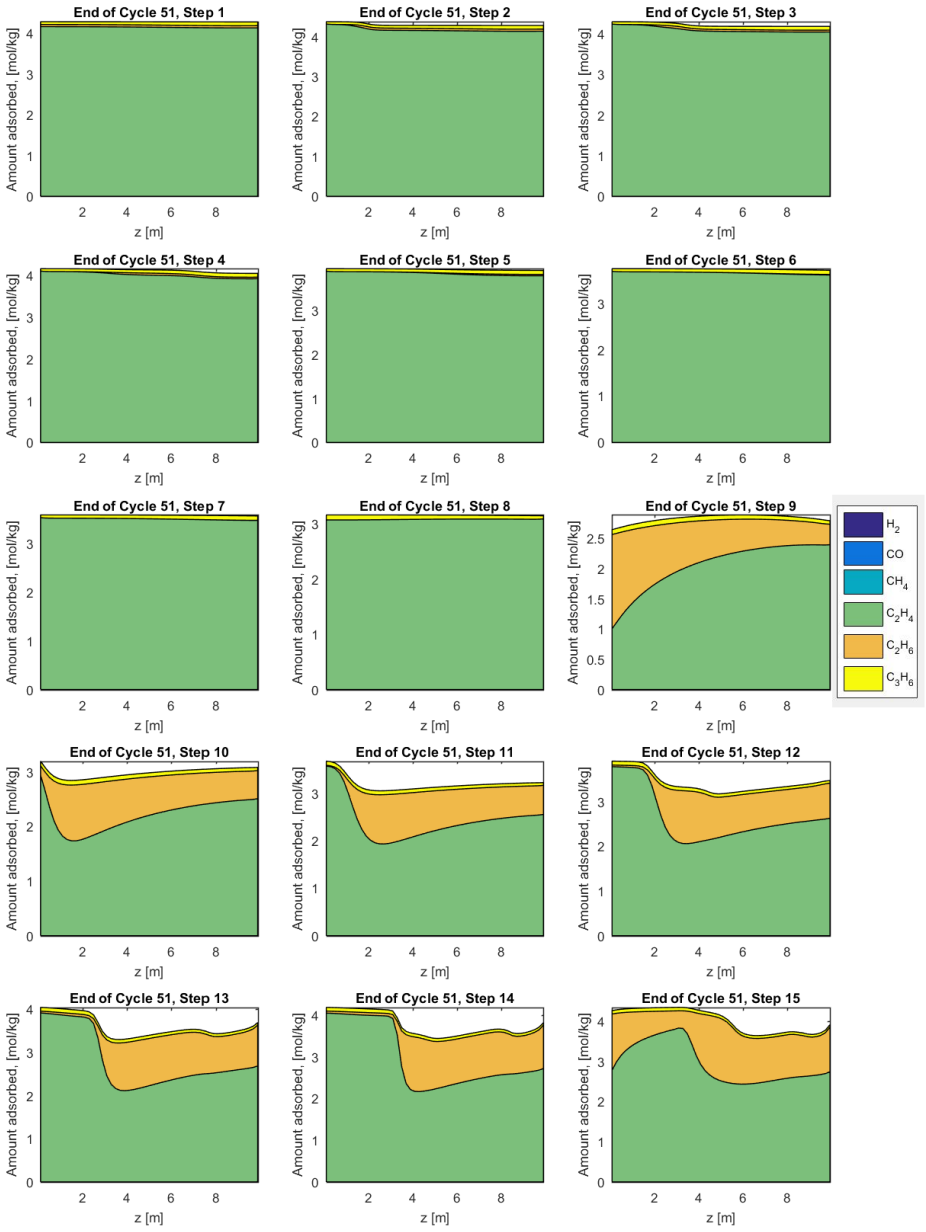


**Figure** 25: Adsorbate loading vs axial coordinate at the end of each step during OPERA cycle, conditions in **Table** 23 (1) Adsorption (2) Rinse (3) Pressure equalisation 1 (4) Pressure equalisation 2 (5) Pressure equalisation 3 (6) Pressure equalisation 4 (7) Pressure equalisation 5 (8) Depressurisation (9) Purge (10) Pressure equalisation 5 (11) Pressure equalisation 4 (12) Pressure equalisation 3 (13) Pressure equalisation 2 (14) Pressure equalisation 1 (15) Repressurisation

# 4

# Conclusions & Recommendations

In this report, a pressure swing cycle is proposed as an alternative to the energy intensive cryogenic distillation process for the separation of Ethylene ($C_2H_4$) from Ethane ($C_2H_6$) and Propylene ($C_3H_6$). The proposed cycle has been developed using the Zeolite 13X sorbent based isotherm for adsorption of $C_2H_4$ over $C_2H_6$ and $C_3H_6$. It has been shown that it is possible to produce high purity $C_2H_4$ using Pressure Swing Adsorption process. A parameter study has yielded an OPERA cycle that produce 99.7 wt.% purity $C_2H_4$ product with 19 wt.% recovery.

In order to further improve the purity and recovery of $C_2H_4$ products the following recommendations are proposed:

## 4.1 Vacuum Pressure Swing Adsorption

Instead of operating between 30 bar and 1 bar, a Vacuum Pressure Swing Adsorption cycle can be designed to operate between 1 bar and 0.1 bar. This greatly increases the recovery of the product as the adsorption isotherm slope for Zeolite 13X is much steeper between 1 bar and 0.1 bar than between 30 bar and 1 bar. The energy needed to operate the cycle at vacuum pressure can be achieved by using the energy attained by expansion of the feed gas from 30 bar to 1 bar. Also, there is no need to pressurise the rinse gas.

## 4.2 Sorbent with different shape

Instead of using spherical sorbent particles, the cycle could be run with sorbents having different shapes possessing higher surface area for the same volume of adsorbent used. This can increase the product recovery considerably for the same amount of adsorbent.

## 4.3 Different sorbent material

Instead of Zeolite 13X, a sorbent should be developed with the following characteristics:

1. Higher selectivity of $C_2H_4$ over $C_2H_6$ which increases the product purity.
2. Adsorption isotherm with higher working capacity between the operating pressures which increases the recovery of the product.

Considering the two characteristics, higher importance should be given for selectivity over working capacity as it is of prior importance to achieve higher purity. The recovery could also be improved by controlling some process parameters.

# Nomenclature

$a_p$ = particle interfacial area per unit volume, $m^{-1}$

c = concentration in gas phase, mol $l^{-1}$

$d_p$ = particle diameter, m

$d_c$ = column internal diameter, m

$d_{crystal}$ = crystal diameter, m

$D_m$ = Molecular diffusivity, $cm^2\ s^{-1}$

$D_k$ = Knudsen diffusivity, $cm^2\ s^{-1}$

$D_z$ = axial mass dispersion coefficient, $m^2\ s^{-1}$

$D_p$ = effective intra particle molar diffusion coefficient, $m^2\ s^{-1}$

$E_a$ = activation energy for surface diffusion, J $mol^{-1}$

$D_c$ = micro pore diffusivity, $m^2\ s^{-1}$

f = friction factor, dimensionless

$F_m$ = mass flow rate, mol $s^{-1}$

i = species index, dimensionless

$k_{LDF}$ = linear driving force intra particle mass transfer coefficient, $s^{-1}$

L = column length, m

M = molar mass, kg $mol^{-1}$

N = molar flux, mol $m^{-2}\ s^{-1}$

N = total number of species, dimensionless

P = pressure, Pa

p = partial pressure, Pa

q = adsorbed phase concentration, mol $kg^{-1}$

$q^*$ = equilibrium value of q

$r_p$ = pore radius, cm

R = gas constant, J $mol^{-1}\ K^{-1}$

t = time, s

T =temperature, K

$T_{wall}$ = wall temperature, K

u = superficial gas velocity, m $s^{-1}$

v = interstitial gas velocity, m $s^{-1}$

z = axial coordinate, m

Greek

α = relative volatility

$\epsilon_b$ = bed porosity, dimensionless

$\epsilon_b$ = particle porosity, dimensionless

ω = mass fraction, dimensionless

ρ = gas density, kg $m^{-3}$

$\rho_p$ = particle density, kg $m^{-3}$

Ω = collision integral

σ = constant in the Lennard-Jones potential energy function

Abbreviations

OPERA = Olefin from Paraffin Extraction by Reversible Adsorption

PSA = pressure swing adsorption

VPSA = vacuum pressure swing adsorption

DSL = Dual Site Langmuir

LDF = Linear Driving Force

CAPEX = capital expenditure

OPEX = operational expenditure

# References


[1] Boon, J., Cobden, P. D., van Dijk, H. A. J., Hoogland, C., van Selow, E. R., & van Sint Annaland, M. (2014). Isotherm model for high-temperature, high-pressure adsorption of CO2 and H2O on K-promoted hydrotalcite. *Chemical Engineering Journal*, *248*, 406-414.

[2] Poling, B. E., Prausnitz, J. M., & O'connell, J. P. (2001). *The properties of gases and liquids* (Vol. 5). New York: McGraw-Hill.

[3] Cheah, S. (2000). *Separation Processes*. Retrieved from www.separationprocesses.com

[4] Do, D. D. (1998). *Adsorption analysis: equilibria and kinetics* (Vol. 2). Imperial College Press.

[5] Ruthven, D. M., Farooq, S., & Knaebel, K. S. (1994). *Pressure swing adsorption* (Vol. 480). New York: VCH publishers.

[6] Narin, G., Martins, V. F., Campo, M., Ribeiro, A. M., Ferreira, A., Santos, J. C., ... & Rodrigues, A. E. (2014). Light olefins/paraffins separation with 13X zeolite binderless beads. *Separation and Purification Technology*, *133*, 452-475.

[7] Boon, J., Cobden, P. D., van Dijk, H. A. J., & van Sint Annaland, M. (2015). High-temperature pressure swing adsorption cycle design for sorption-enhanced water–gas shift. *Chemical Engineering Science*, *122*, 219-231.

[8] Khajuria, H. (2011). *Model-based Design, Operation and Control of Pressure Swing Adsorption Systems* (Doctoral dissertation, Imperial College London (University of London)).

[9] Van Miltenburg, A. (2007). *Adsorptive separation of light olefin/paraffin mixtures: dispersion of CuC1 in Faujasite zeolites*. TU Delft, Delft University of Technology.

[10] Ruthven, D. M. (1984). *Principles of adsorption and adsorption processes*. John Wiley & Sons.

[11] Silva, F. A. D., & Rodrigues, A. E. (2001). Propylene/propane separation by vacuum swing adsorption using 13X zeolite. *AIChE journal*, *47*(2), 341-357.

[12] Jain, S., Moharir, A. S., Li, P., & Wozny, G. (2003). Heuristic design of pressure swing adsorption: a preliminary study. *Separation and Purification Technology*, *33*(1), 25-43.

[13] *Slideshare.* (2010). Retrieved from http://www.slideshare.net/cxmStrawberry/industrial-uses-of-ethene

[14] Thomas, W. J., & Crittenden, B. D. (1998). *Adsorption technology and design*. Butterworth-Heinemann.

[15] Yang, R. T. (2013). *Gas separation by adsorption processes*. Butterworth-Heinemann.

**ECN**
Westerduinweg 3
1755 LE  Petten
The Netherlands

P.O. Box 1
1755 LG Petten
The Netherlands

T +31 88 515 4949
F +31 88 515 8338
info@ ecn.nl
www.ecn.nl